New direction for earth reinforcement: disaster prevention for earthfill dams

Y. Mohri[1], K. Matsushima[2], S. Yamazaki[3], T. N. Lohani[4], F. Tatsuoka[5] and T. Tanaka[6]

[1]*Chief of Geotechnical Engineering Laboratory, Department of Geotechnical and Hydraulic Engineering, National Institute for Rural Engineering, 2-1-6, Kan-nondai, Tsukuba, Ibaraki 305-8609, Japan, Telephone: +81 29 838 7574, Telefax: +81 29 838 7609, E-mail: ymohri@affrc.go.jp*
[2]*Research Engineer, Department of Geotechnical and Hydraulic Engineering, National Institute for Rural Engineering, 2-1-6, Kan-nondai, Tsukuba, Ibaraki 305-8609, Japan, Telephone: +81 29 838 7575, Telefax: +81 29 838 7609, E-mail: kenichim@affrc.go.jp*
[3]*Research Engineer, Mitsui Chemicals Industrial Products Ltd, Kawaraicho 9, Kukishi, Saitama, Japan, 346-0028, Telephone: +81 480 28 2071, Telefax: +81 480 28 2072, E-mail: s_yamazaki@mitsui-sanshi.co.jp*
[4]*JSPS Post-Doctoral Fellow, Department of Architecture and Civil Engineering, Kobe University, 1-1 Rokkodai-cho, Nada-ku, Kobe City, Kobe, 657-8501, Japan, Telephone: +81 78 803 6812, Telefax: +81 78 803 6069, E-mail: tnlohani@gmail.com*
[5]*Professor, Department of Civil Engineering, Tokyo University of Science, 2641, Noda, Chiba, 278-8510, Japan, Telephone: +81 4 7122 9819, Telefax: +81 4 7123 9766, E-mail: tatsuoka@rs.noda.tus.ac.jp*
[6]*Professor, Department of Biological and Environmental Engineering, University of Tokyo, 1-1-1, Yayoi, Bunkyo-Ku, Tokyo, Japan, Telephone: +81 3 5841 5346, Telefax: +81 3 5841 8170, E-mail: atanak@mail.ecc.u-tokyo.ac.jp*

Received 25 April 2008, revised 22 December 2008, accepted 25 December 2008

ABSTRACT: A large number of geosynthetic-reinforcing technologies for embankments and retaining walls have been proposed and developed, and the behaviour of these structures has been evaluated using laboratory tests and field tests, as well as full-scale case histories. Yet a great number of embankments have failed in Japan owing to strong seismic loads and heavy rainfall. Significant improvements are required in the construction of earthfill dams to prevent these failures. This paper reviews the characteristic features of the damage to small earthfill dams that has taken place during earthquakes as well as heavy rainfall. The paper then describes a new technology using geosynthetic soil bags with extended tails stacked on the downstream slope to construct earthfill dams that are highly stable against earthquakes as well as heavy rainfall leading to overtopping by flood water. Some fundamental aspects of the stability of embankments reinforced by soil bags and seismic behaviour are examined using static loading, hydraulic breach tests and shaking-table tests.

KEYWORDS: Geosynthetics, Disaster prevention, Soil bags, Earthfill dam, Earthquake, Breaching failure

REFERENCE: Mohri, Y., Matsushima, K., Yamazaki, S., Lohani, T. N., Tatsuoka, F. & Tanaka, T. (2009). New direction for earth reinforcement: disaster prevention for earthfill dams. *Geosynthetics International*, **16**, No. 4, 246–273. [doi: 10.1680/gein.2009.16.4.246]

1. INTRODUCTION

Earthfill dams must withstand two extreme events: major floods due to heavy rainfall, and earthquakes. In Japan there are more than 210 000 small earthfill dams for agricultural irrigation, and almost all are located near cities. Among the small earthfill dams currently operated, 48 000 or more were constructed before AD 1600. These reservoirs have been maintained by regional management organisations for some 200 years, but at least 20 000 of these earth dams are deteriorating with age by leakage and sliding. The body of the dam consists of soil materials, so there is a possibility that slight erosion on the slope of the dam caused by rainfall may gradually develop into a large-scale collapse. In addition, there have been many reports of dam bodies damaged by an earthquake that have failed unexpectedly.

Figure 1 shows the cumulative and annual numbers of damaged small earthfill dams in Japan, from 1976 to 2004. The figure shows that complete dam failure occurs

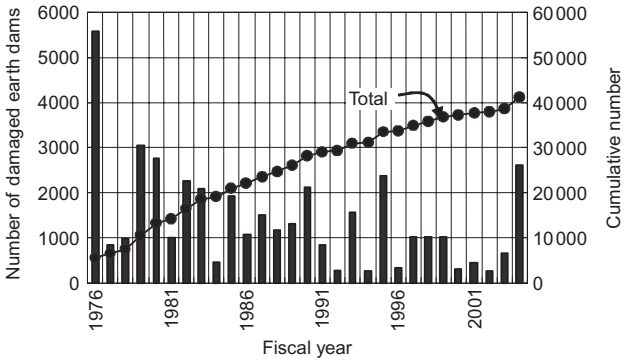

Figure 1. Annual and cumulative numbers of damaged small earthfill dams in Japan. 1995 data include 1200 sites damaged by the Hyogoken-Nanbu earthquake; 2004 data include 561 sites damaged by the Niigataken-Chuetsu earthquake.

several times a year, but most small earthfill dams have been damaged by sliding and leakage. It is obvious that many dams were damaged by severe seismic loading during the 1995 Hyogoken-Nanbu earthquake and the 2004 Niigataken-Chuetsu earthquake, but over 300 dams were adversely affected by slip failure of embankment and overflow caused by rainfall every year.

These small earthfill dams are usually reconstructed to the original condition and structural type, even though the reconstructed dam may suffer the same damage again when subjected to an earthquake or rainfall of the same level.

However, considering that localised torrential rain exceeding 1000 mm daily often occurs throughout Japan, causing unexpected flooding, and that earthquakes occur frequently, it is essential to develop a small earthfill dam of high durability.

Breaching issues related to earthfill dams due to overflow by heavy rainfall have been addressed in many reports at previous symposiums of the International Commission on Large Dams (ICOLD), and some hydraulics journals. A general report presented by Tournier (2006) provided an extensive review of dam safety, breaching, evaluation of risk, and rehabilitation.

Geotextile containment has been used for many years in order to prevent the erosion and collapse of earth embankments or foundations in hydraulic and marine applications. Lawson (2008) provided a detailed review of the three main geotextile containment units in use: tubes, containers and bags. Various interesting case histories have been reported by Leshchinsky *et al*. (1996), Ghazali *et al.* (2006) and Cho *et al*. (2008).

Soil bags have been used to protect dykes and to reinforce foundations against floods or earthquake. Examples of their use have been reported by Kim *et al.* (2004), Xu *et al.* (2008) and Chen *et al*. (2008). Matsuoka *et al*. (2003) and Lohani *et al*. (2006) indicated that the bearing capacity of foundations can be increased by using a soil bag or stacked soil bags. The shear properties of stacked soil bags were reported by Krahn *et al.* (2007), Matsuoka *et al.* (2003) and Matsushima *et al.* (2008). Regarding the stability of stacked soil bag slopes, Huang *et al.* (2008) reported that the results of limit equilibrium analyses showed good agreement with the results of small physical model tests.

Krahn *et al*. (2007) addressed the results of a large direct shear test of a sandbag dyke for a flood protection structure. The tests results showed that the shear strength of sandbag dyke interfaces is greater than that deduced from interface shear testing on sandbag geotextile sheets. The dilatant behaviour of sandbags during large shear deformation had a considerable effect on the strength of the stacked layers, but reinforcing technology or a modification of the layer system of sandbags was needed to prevent slip failure at the interface. However, they did not show any specific technology using sandbags for protection.

Tatsuoka *et al*. (2007) addressed the advantages of geosynthetic reinforcing technology for new soil structures. Geosynthetic structures such as embankments, soil-retaining walls and earth fills have a higher stability against seismic load and rainfall, based on experiments on serious damage to civil engineering structures. Maruyama *et al.* (2006) described rehabilitation work for an earthfill dam in Tokyo using geosynthetic reinforcing technology, in which a planar geosynthetic was installed in the embankment. The existing dam, the Shimo-Murayama dam, was rehabilitated by stabilising the downstream slope, aiming at a substantial increase in the seismic stability.

No paper can be found in the literature that reports any type of reinforcing technology that is useful for both erosion protection and seismic resistance for earthfill dams.

There is a real need to develop a technique to prevent frequent damage to earthfill dams and avoid related disasters. The authors are engaged in a research project with the ultimate aim of developing a high-durability earthfill dam that is secure against both overflow and earthquake. In this paper several cases in which conventional earthfill dams were either damaged failed totally as a result of heavy rainfall and serious earthquake are described, in order to clarify the key causes. Then a geosynthetic reinforcing technology with high resistance against both water flow and earthquake action is reported. Finally, test results are described for the breaching and seismic performance of the new type of earthfill dam, in which stacked soil bags are used to increase either the downstream slope or both side slopes of an old earth dam.

2. CASE HISTORIES OF SMALL EARTHFILL DAMS

2.1. General

It is first necessary to understand the detailed destruction patterns of small earthfill dams and their mechanisms in order to develop innovative technologies to improve the durability of the dams.

These dams exhibited several destruction patterns due to heavy rainfall. The main causes of destruction can be classified into three types, as shown in Figure 2: failure by overflow, failure by sliding, and failure by internal erosion. The combination of these causes and multiple conditions that destroy the body of the dams must also be considered, but it is also useful to analyse respective damage cases

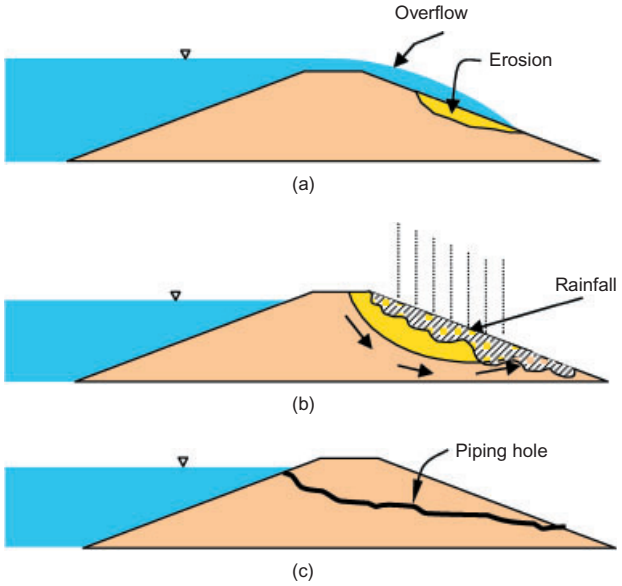

Figure 2. Three modes of dam failure after heavy rainfall (after Hori *et al.* 1998): (a) overflow; (b) sliding failure; (c) seepage

when developing technologies to prevent destruction. The dams must be able to withstand individual destruction patterns fully in order for the overall safety of the dam body to be enhanced. These damage patterns can be classified as shown in Table 1.

A failure by overflow is an event in which a flood occurs that exceeds a spillway's capacity for discharging the flow in a small earthfill dam. The dam's retained water flows over the crest of the body and erodes the crest surface and downstream slope, thus destroying the embankment. A failure by sliding is an event in which the seepage of water and rainfall into the downstream slope increases the porewater pressure within the embankment and decreases the strength of the body, causing the slope to slide. A failure by internal erosion for an earthfill dam is an event in which fine soil particles are washed away from the embankment by groundwater flow, making a continuous hole in the dyke. These critical areas in the earthfill dam propagate easily from the downstream slope side to the crest or upstream slope side by an increase in the groundwater flow during the heavy rainfall, causing slip failure around these discontinuous planes.

Fujii *et al.* (1991) and Yasunaka and Tagashira (1994) surveyed the case histories of small earthfill dam failures and reported that 30% of small earthfill dams damaged by heavy rainfall in Japan were destroyed by overflow. When failures caused by sliding of the downstream slope were included, this failure rate reached 60%.

2.2. Damage by rainfall

2.2.1. *Failure by overflow*

Water flowing over the body of a small earthfill dam erodes the surface soil of the embankment with its streaming momentum, and progresses to cause head cut failure of embankment. Considering soil erosion caused by flowing water, a cohesive clay slope is more resistant to erosion than a sand slope. However, a larger overflow velocity on the slope has a great influence on the rate of erosion of the slope and the volume eroded, even for a clay slope. The embankment is required to have high resistance to severe overflow, and to be able to remain stable against sliding failure of down stream slope.

Figure 3 shows the state of a small earthfill dam that was destroyed by overflow. Figure 3a shows the condition immediately after the water level rose to the crest surface of the dam, and the erosion of the downstream slope continuing to develop with the start of overflow. If a large-scale flood occurs, or if the natural ground around a reservoir collapses and the water level is increased significantly, the whole embankment can collapse, or it may be partially destroyed when the overflow duration time is short. In any case, the body of the dam does not have great resistance to an overflowing stream, so the erosion of the downstream slope proceeds, reducing the section of the embankment and finally destroying the body. The degree of failure of the embankment depends greatly on the soil materials of the embankment and the paving condition of the upper surface, as well as on the water flow velocity and duration of the overflow.

2.2.2. *Failure by sliding*

The embankment of a small earthfill dam is usually unsaturated before rainfall, and suction in a dyke contributes to stability by increasing the confining pressure of the fill material. As the embankment's water content increases by seepage or rainfall, its suction and shear resistance decrease, and its lowered resistance increases the risk of failure by sliding. Most sliding events on an embankment during heavy rainfall occur at the downstream slope. Continuous rainfall gradually infiltrates the embankment, thereby increasing the degree of ground saturation. At the same time, the groundwater table generated by seepage into the body also rises, in a staged manner. For this reason, as the pore pressure within the embankment increases, the downstream slope decreases in

Table 1. Destruction patterns of the body of small earthfill dams

Category	Events or causes
Overflow	Flood, small embankment height
Sliding	Increase of upstream water level, seepage into embankment, and rising groundwater level around the toe end of downstream slope
Internal erosion	Piping route, sink fall, soil pressure decline on the outlet conduit by arch action within the embankment

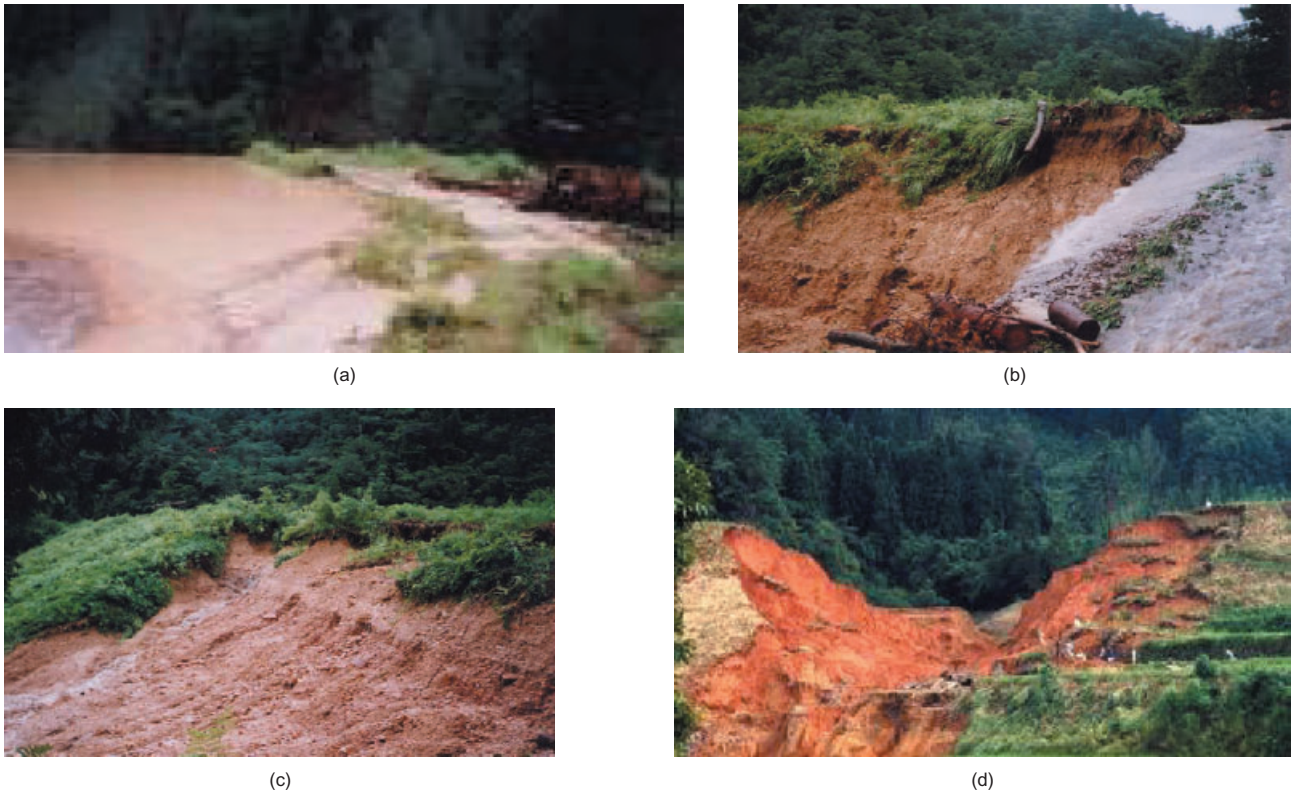

Figure 3. Erosion of downstream slope by overflow and progression into failure of slope: (a) upstream water level; (b) overflow; (c) downstream slope failure by sliding; (d) total failure

strength, resulting in sliding collapse. The causes of slope failure by sliding resulting from this rainfall include:

- reservoir water level conditions;
- embankment geometry (slope gradient);
- embankment soil conditions (permeability coefficient, water retention properties, cohesion, internal friction angle, etc.)

When rehabilitating an existing old earthfill dam, it is most effective to install a drain at the toe of the downstream slope. If this drain lowers the groundwater table in the dyke, it will prevent the reduction of strength of the sliding body, thus significantly increasing the safety factor. In addition, it is also effective to cover the surface of the downstream slope with an impermeable layer and directly reduce the infiltration of rainfall into the body.

2.2.3. *Key factors for rehabilitating existing old earthfill dams*

For failure by overflow, it is necessary to develop a slope reinforcement method that can prevent immediate destruction of the body of an existing old earthfill dam even if the dam water overflows the embankment. It is also necessary to develop a method for evaluating the structural safety of the body that allows for overflow.

For failure by sliding, it is important to control rainfall seepage and take measures against erosion in order to maintain the mechanical safety of the downstream slope. In addition, a drain to maintain the embankment's saturation line at a safe level is very effective and economical.

2.3. Damage by earthquake

2.3.1. *Damage to dyke*

In the 1995 Hyogoken-Nanbu earthquake that struck the Kobe area of Japan, even the agricultural infrastructure was also seriously affected, including earthfill dams, land reclamation embankments and farm roads. For large-scale earthfill dams designed using modern soil mechanics technology, even this large earthquake caused only very slight damage, but small earthfill dams for irrigation suffered serious damage, including total failure and sliding.

Figure 4 shows a damaged small earthfill dam, in which the whole dam dyke underwent large settlement, owing to widespread liquefaction of the foundation below the dyke.

Figure 4. Total failure and large settlement caused by Kobe earthquake, due to liquefaction (Hyogo Pref. 1996)

The crest of the dam settled about 5 m during the earthquake, and many soil boils were found around the dyke. Figure 5 shows slip failure on the upstream slope of a small earthfill dam that consisted of clay materials.

When a small earthfill dam is hit by an earthquake, it vibrates greatly along the dam axis and in the perpendicular direction. As a result, tension cracking occurs near the crest surface of the embankment, causing shear failure within the body. If the embankment is seriously shaken, the deformation caused by these failures accumulates, resulting in a large sliding collapse. When the dam retains water and is struck by an earthquake, it may cause a large sliding collapse downstream under water pressure. If the foundation of the dam is soft or undergoes liquefaction, as reported by Tani (1996), often the whole body settles down and collapses completely.

The factors that affect the destruction of the embankment in an earthquake include:

- the strength of embankment, and the soil conditions;
- the properties of the foundation;
- the earthfill dam geometry (slope gradient);
- the magnitude and duration of earthquake ground motion.

Because of the motion of the embankment during an earthquake, its crest surface is often cracked. As shown in Figure 6, several continuous cracking events parallel to the embankment axis can occur. These surface cracks may extend to the depth of the embankment, even if the opening width of the surface is only approximately 0.05 m. In one small earthfill dam hit by the 1995 Hyogoken-Nanbu earthquake, cracks reached the bottom of the impermeable core layer, as shown in Figure 7, so the entire dam had to be excavated to reconstruct a new embankment. In cases where slope sliding as well as cracking is caused by an earthquake, larger cracking occurs on the crest surface, and such a damaged dam will require large-scale rehabilitation, including the slope.

Figure 5. Upstream slope sliding by seismic loading (Hyogo Pref. 1996)

Figure 6. Open crack in direction parallel to dam axis (Hyogo Pref. 1996).

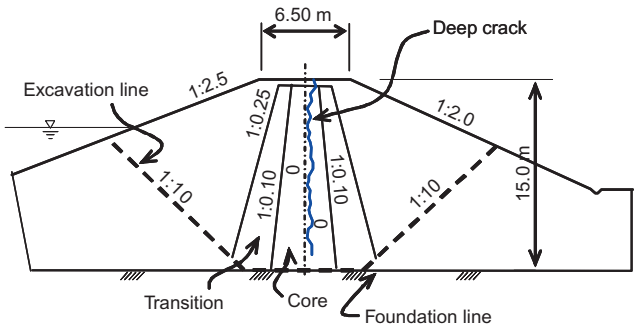

Figure 7. Crack propagating to bottom of core zone from crest (Hyogo Pref. 1996)

3. DEVELOPMENT OF A NEW CONSTRUCTION METHOD FOR OVERFLOW-TOLERANT AND EARTHQUAKE-RESISTANT SMALL EARTH DAMS

3.1. General

Existing old earthfill dams consist of an earth embankment and a concrete spillway. When such dams were designed, relevant seismic loads due to earthquakes were usually not taken into consideration. Also, because almost all old earthfill dams were constructed before the design standard for spillway capacity, which was revised in order to provide safe discharge water flow by the spillway even in heavy flood conditions, many dam spillways have insufficient capacity to discharge the water of occasional heavy floods.

Many small earthfill dams for agricultural irrigation have been seriously damaged or have completely failed by

overflow during typhoon-induced flooding that exceeds the drainage capacity of the spillway discharge system, or during earthquakes. This natural hazard of overflow can totally destroy downstream city areas, so a new method is needed for constructing small earthfill dams that can tolerate both overflow due to flooding and the seismic loads of earthquakes.

It is very expensive to increase the drainage capacity of the flood discharge spillway system of a reinforced concrete (RC) structure so that it can discharge the design flood that might only take place once every 200 years. Moreover, a large spillway system on a small earthfill dam requires reinforcement of the dam dyke itself around the spillway in order to increase the strength of the dam, and prevent rupture of the embankment. This rehabilitation approach is not cost-effective, and the construction work takes too long.

Geosynthetic reinforcement technology is receiving increasing attention in the civil engineering community, because it can provide cost-effective solutions to several critical construction and maintenance problems of civil engineering structures, sometimes combined with other new construction technologies. Horizontal arrangement of planar sheets of geogrid or geotextile made of polymer embedded in the backfill is one of the most popular soil-reinforcing technologies. The use of soil bags made of polymer geosynthetic is another technology for reinforcing foundations and embankments, because soil bags can exhibit relatively large compressive strength when vertically compressed, without external confinement.

Mohri *et al.* (2005) proposed protecting the downstream slope of such earthfill dams by using soil bags anchored with geosynthetic reinforcement layers arranged inside the slope, as shown in Figure 8. This is a realistic, cost-effective and simple method for rehabilitating a large number of old earthfill dams without increasing the capacity of an existing flood discharge RC structure.

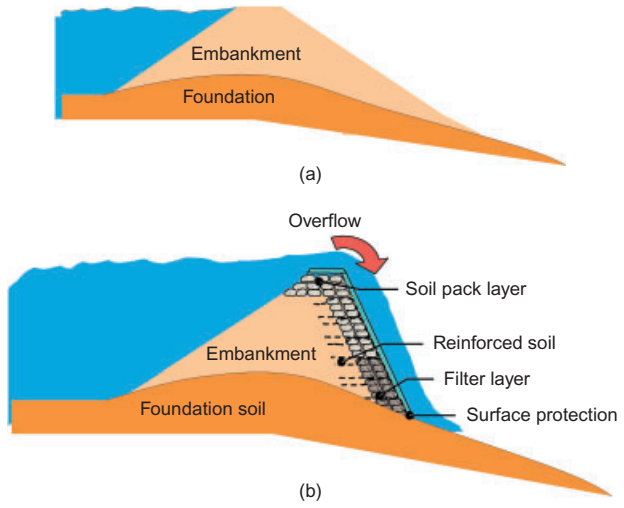

Figure 8. New technology to rehabilitate existing old earthfill dams to have high flood discharge capacity and high seismic stability (after Mohri *et al.* 2005): (a) existing earthfill dam; (b) using soil bags

Moreover, the slope constructed or reconstructed by the new technology is more stable against seismic load.

In the new construction method for small earth dams, the dam section is a composite structure of earthwork: an impermeable core zone constructed of clay, geosynthetic soil bags with extended tails (GSET) filled with appropriate backfill material, and a geosynthetic wing. The use of advanced soil bags not only increases stability against overflow but also provides resistance against earthquake-induced forces.

3.1.1. *Performance for GSET*

Soil bags in this application are required to have particular qualities and performance in order to prevent severe damage of embankments by overflow water in flood and earthquake excitation. Therefore the GSET is different from the small soil bags used for temporary protection, in terms of its size and mass, and the bag material. The GSET as a stacked soil bag structure offers performance advantages against both events, as follows:

- high stability against seismic loads due to the geosynthetic reinforcement;
- a dam with stacked soil bags can tolerate overflow;
- the existing spillway can also be used as an emergency spillway during floods.

3.1.2. *Efficient, cost-effective construction method for GSET*

A GSET embankment is also different from the original structural type used for existing earthfill dams (e.g. embankments having a gentle slope, and only soil being used for the dyke). It can be characterised as follows.

- It is cost-effective, because there is no need to build an additional spillway (and hence construction is faster).
- No heavy equipment is needed, so construction in remote locations is possible.
- The reduced base width and top crest require less in terms of earthworks (e.g. a narrow space, or a steep slope).

3.2. Earthfill dams stabilised by geosynthetic soil bag system with extended tail (GSET dam)

The GSET dam is a method for piling up soil bags as shown in Figure 9 to construct an earthfill dam that has higher stability even when a flood causes overflow of the embankment. This soil bag, which has a flat shape with an aspect ratio of 5 to 8, consists of a large soil bag with a mass of 2 kN or more, and a tail and a wing that are connected to the main. The wing is inserted between neighbouring soil bags, thereby ensuring the strength of stacked soil bags serving as a potential wall. The tail is installed within the embankment, so it exerts a reinforcement effect in combination with the stacked soil bags and embankment. The body of the soil bag system and the tail reinforce a wider area of the embankment, and increase the strength of the whole body as a flexible wall. Furthermore, as the materials within the soil bag are

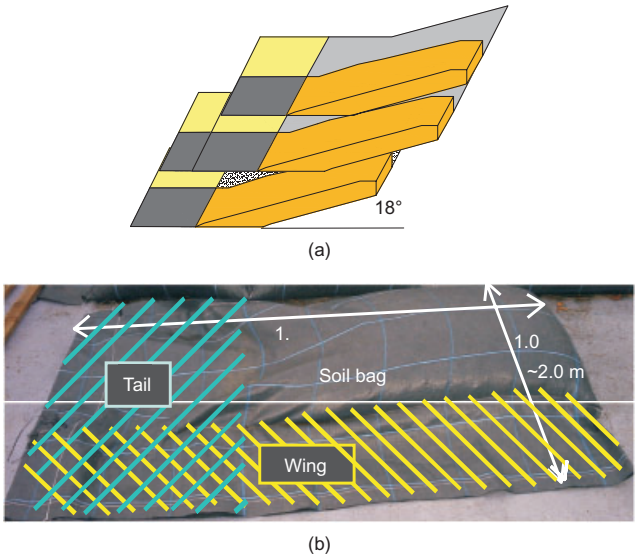

Figure 9. Geosynthetic soil bag with extended tail and inclined stacking system: (a) inclined stacking; (b) GSET

confined by the bag and exert a larger bearing capacity, on-site soil of low quality can be used. When high-permeability materials such as crushed stone are used for the embankment, its stacked layer can also serve as a drain. Therefore these materials provide resistance to overflow, and also improve measures against leakage and the safety of the dam during an earthquake.

It is important to evaluate the soil bag strength for full use of the capability of the soil bag system in stabilising the structure of stacked soil bags. The compressive properties of soil bags were reported by Matsuoka *et al*. (2001) and Lohani *et al*. (2004). Regarding the shear resistance of stacked soil bags, Aqil *et al*. (2005, 2006) and Matsushima *et al.* (2008) reported the results of a large-scale shearing test. It is difficult to ensure sufficient resistance by simple vertical compression tests of vertically stacked soil bags, because sliding friction between soil bag materials is small, and friction dominates the shear deformation of the whole stacked body. For this reason, Matsushima *et al*. (2008) suggested increasing the shear resistance of the body by installing soil bags at a inclined angle, and they provided detailed data on the increased resistance.

4. OVERFLOW REGIMES OF GSET DAM

4.1. Hydraulic flow regimes and erosion

The mechanics of embankment erosion during overflow have been widely documented in the literature, for example for the numerous small earthfill dam failures that occurred in the 1960s. The observations of Ralston (1987) and Powledge *et al.* (1989a) indicate that headcut formation and advance are critical processes in breach of embankment dams. The mechanics of headcut erosion, causing breach of an earth spillway, were discussed in detail by Temple (1989).

For cohesive soil embankments, breach takes place by headcutting. In general, a first, small headcut forms near the toe of the dam, and then progresses to the upstream side until the crest of the dam is breached, as shown in Figure 10. A series of stepped headcuts forms on the downstream face of the dam. Dodge (1988) reported on the results of early tests in which overtopping flows were simulated over model embankment dams. The tests were designed to evaluate the effectiveness of various crest and embankment face protection schemes that would permit overflow without causing dam breach.

Powledge *et al*. (1989b) described three hydraulic flow regimes and erosion zones for embankment overflow. In the flow region on the dam crest, the velocities and tractive stress are relatively low, and no significant erosion will occur. On the downstream portion of the crest, the energy slopes and traction stress are higher, and erosion is sometimes caused at the knick point at the downstream edge of the crest. Another point of erosion is the downstream face of the dam. Tractive stresses are very high, and changes in slope or surface discontinuities cause the stress to concentrate, thereby initiating erosion.

Erosion may start at any point on the slope, but the toe is the most common location. Once erosion has been initiated, a headcutting behaviour is generally observed, in which the scour hole moves upstream and widens.

4.2. Stream regimes of stepped spillways

A GSET dam with stacked soil bags as shown in Figure 11 can be considered as one specific type of stepped spillway. Because of its high energy-dissipating effect, such a stepped configuration has been widely used for concrete dams. A number of researchers have already

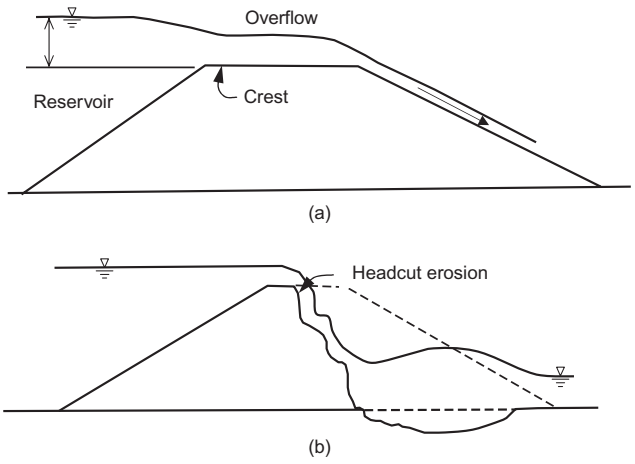

Figure 10. Progressive headcutting breach of cohesive soil embankment (after Powledge *et al*. 1989b): (a) just after overflow; (b) after failure

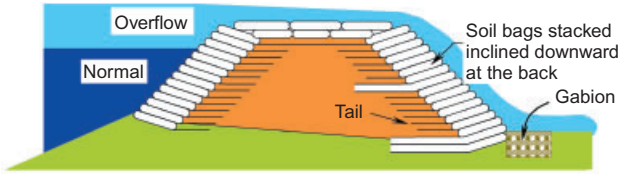

Figure 11. Basic components of GSET spillway for temporary flooding (after Matsushima *et al.* 2008)

studied the overflow characteristics of such dams (Hubert 1994). The overflow characteristics can be classified into the following three main types, as shown in Figure 12, depending on the step height, the discharge and the slope of the spillway:

- nappe flow, characterised by the formation of a nappe and an air pocket at each step (Figure 12a);
- skimming flow, characterised by the formation of an eddy at each step (Figure 12b);
- the formation of free fall at the top of the slope (Figure 12c).

However, no study on the influence of such regimes on the stability of a GSET dam against overflow has been performed. Figure 13 shows a conceptual illustration of the damage mechanisms, as a function of overflow level, that may affect the stability of a GSET dam subjected to overflow. The damage mechanisms of the GSET dam against overflow are controlled by the following three damage mechanisms of the downstream slope:

- suction of backfill material by negative pressure, that is, washout of soil particles from the embankment through spaces between the soil bags;
- attrition of geosynthetics by tractive force;
- breakage of geosynthetics by penetration force caused by free water fall.

To evaluate the stability of GSET dams against overflow affected by these three damage mechanisms, a series of large-scale model hydraulic overflow failure tests was conducted. Based on observations of the tests, the damage patterns on the GSET dam were identified, and categorised as a function of the different stream regimes that depend on overflow levels.

5. PHYSICAL BREACH TESTS FOR SOIL BAG SYSTEM

5.1. Small-scale breach tests for soil bag system

An overlain downstream slope covered by impermeable materials such as geosynthetics, gabions and concrete blocks should have a high resistance to overflow during a flood. However, if the overflow passes into the dyke under the surface layer, the downstream slope may suffer severe erosion as the advance rate drastically increases. To validate the above, and confirm the behaviour of the soil bag facing system on the slope during overflowing, a series of model tests was performed. Six small models with different facing arrangements, as listed in Table 2, were prepared. The model consisted of a 200 mm-thick base ground, on which a 500 mm-high model earthfill dam with a slope of 1V:2H on a scale of 1/10 of an assumed prototype was constructed, as shown in Figure 14a. The fill material is Hokota sand (specific gravity, $G_s = 2.676$; mean diameter, $D_{50} = 1.84$ cm; coefficient of uniformity, $U_c = 5.82$; maximum dry density, $\rho_{dmax} = 15.17$ kN/m^3; and optimum water content, $w_{opt} = 14.3\%$), compacted at water content $w = 1.1.5\%$ to a relative density D_r equal to 85% (not very dense). The soil bags were made of polyester. With this model, the water flow was continued while increasing the flow rate every hour, as shown in Figure 14a.

Figure 14a also illustrates the stream line on the slope at the constant flow rate in the cases where the slope may suffer failure by washing out of the slope surface, and the depth of overflowing water at the crest. Figure 14b shows that protecting the slope surface by using GSET with sufficient overlap between vertically adjacent soil bags (cases 3 to 6) increases the stability against overflow in comparison with cases 1 and 2. The first phase of failure of a slope embankment by overflow is initial failure of the protective cover on the downstream face of the fill. Of

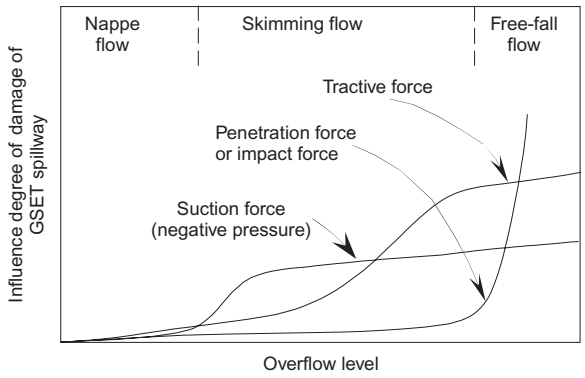

Figure 13. Damage mechanism of GSET spillway as a function of overflow level

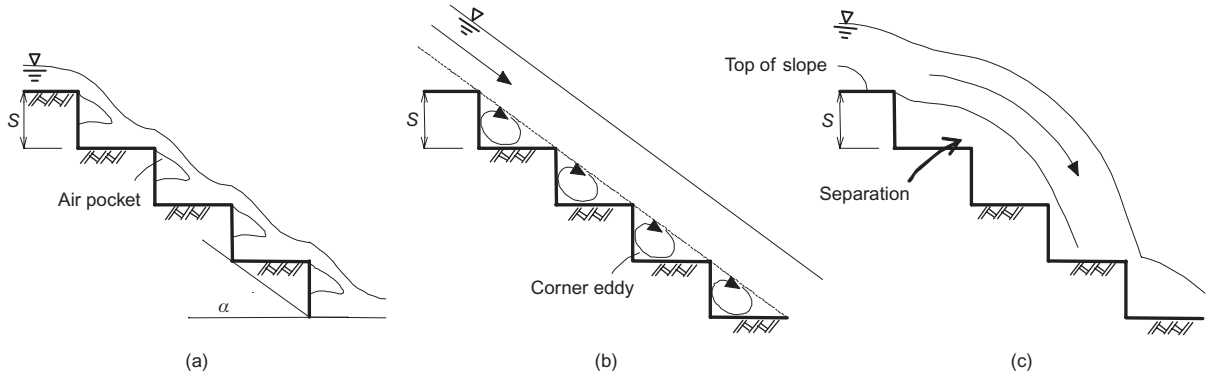

Figure 12. Stream regimes of stepped spillways (after Hubert 1994): (a) nappe flow; (b) skimming flow; (c) free-fall flow

Table 2. Small-scale breaching tests cases (Matsushima *et al.* 2005)

Case	Slope protection	Soil bag dimensions (thickness × width × length, mm)
1	Nonwoven	Sheet
2	Type A soil bags without overlapping	20 × 50 × 60
3	Type A soil bags with overlapping	20 × 50 × 60
4	Type B soil bags with overlapping	25 × 80 × 80
5	Type C soil bags with overlapping	20 × 80 × 120
6	Type D soil bags with overlapping	20 × 50 × 180

course, a higher velocity and higher turbulent flow over the slope face may induce more rapid erosion of the facing materials.

The failure patterns after breaching tests and the mechanical behaviour for individual models (cases 1 to 6) are described below.

- Case 1: The slope soil was eroded gradually with time as water flowed below the nonwoven geosynthetic sheets, finally resulting in a sudden shallow failure of the slope.
- Case 2: The slope was protected by placing the soil bags on the slope surface with no overlapping between vertically adjacent soil bags. Sliding failure between the slope and the soil bags occurred by water flowing into the interface, even when the flow rate was still low.
- Cases 3: The slope was protected by placing the soil bags overlapping vertically, with an overlap length of about 20 mm. This slope type was not eroded by flowing water level I (indicated in Figure 14). However, after rising up to the second flowing water level, the cover layer with soil bags was washed out by the flow, because water entered the interface between the soil bags and the slope.
- Case 4: This type, which had a longer overlap (30 mm) than Case 2, suffered no damage at the

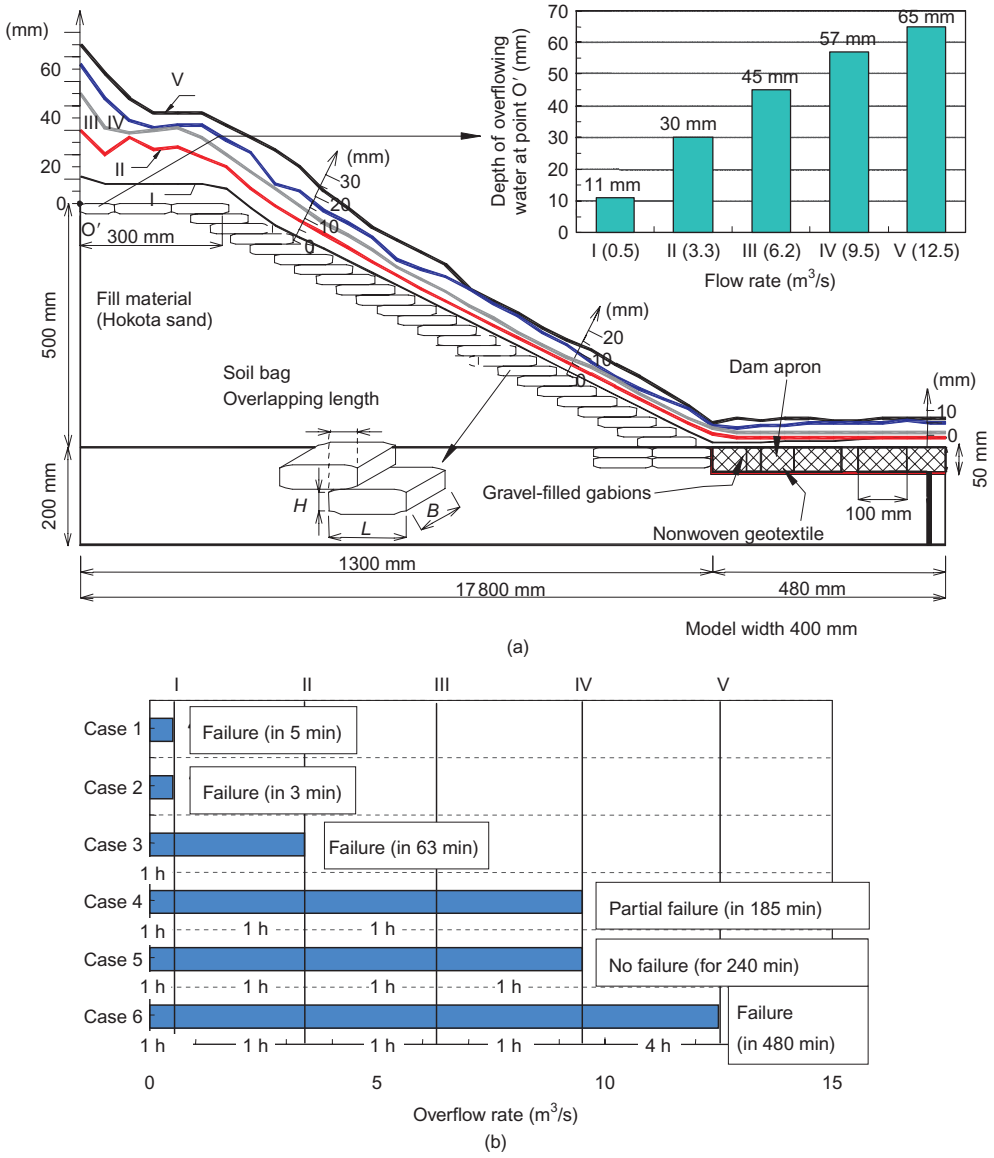

Figure 14. Overflow line and results for small-scale breaching tests (after Yamazaki *et al.* 2006): (a) depth level of flowing water; (b) flow level

third water level. Some soil bags around the centre level were pulled out suddenly, and the slope toe failed by washing out of the soil bags.

- Cases 5 and 6: By using longer soil bags with a larger overlap (80 mm and 140 mm) between vertically adjacent bags, the slope became more stable, with less erosion of the slope soil. No rupture occurred in either case at the fourth water level.

5.2. Large-scale breaching tests for GSET dam model

Physical hydraulic model testing may include two-dimensional modelling of earthfill dam sections of the entire dyke, and will help clarify the fundamental mechanism of downstream slope breaching. In order to confirm the overall behaviour of the dyke and the formation of breaching, physical modelling should be performed on a large scale to overcome the problem of simultaneous scaling of both hydraulic conditions and material properties.

Even for a small earthfill dam, it will be difficult to conduct full-scale hydraulic model testing. Despite that, the scale should be sufficiently large to allow the use of prototype embankment materials, soil bags, and backfill materials.

5.2.1. *Experiment models and materials*

The GSET dam model for the breaching test is a 3.5 m high embankment with soil bags used for an actual earthfill dam to conduct a realistic overflow test. As shown in Figure 15, the soil bags are stacked on the upstream and downstream slope faces of the embankment model with a total of 24 soil bag steps to construct a surface that is resistant to overflow. These soil bags were stacked with a 15° angle to the foundation ground in order to increase the shear resistance of the stacked soil bags and enhance the safety of the model. Referring to the results obtained from compression tests, which are described later in this paper, recycled crushed concrete aggregate (RC-40) was used as a backfill material for the soil bags to improve the bags' strength, and establish an embankment model with enhanced overall safety.

This model has a downstream slope of 1V:1.2H and a depth of 2.3 m. Kasama sand (specific gravity, $G_s = 2.65$, maximum dry unit weight, $\rho_{dmax} = 19.35$ kN/m^3; optimum water content, $w_{opt} = 11.6\%$) and a mixture of Kasama sand and a clayey silt (called Kanto loam) (dry unit weight, $\rho_s = 26.16$ kN/m^3; $\rho_{dmax} = 14.7$ kN/m^3; $w_{opt} = 24.6\%$; Kanto loam 1: Kasama sand 1.5 by mass) were used for the embankment and for the core soil, respectively.

PP sheet with a tensile strength of 1.25 kN/m was used for the soil bag material. Unlike a normal large soil bag, this bag basically has a flat shape with a large aspect ratio ($L/H = 5$ to 8). As shown in Figure 9, it has a wing and a tail at its side and rear end, respectively. The wing is inserted into neighbouring soil bags to prevent separation between soil bags, and the tail is buried in the embankment. These two measures help the whole soil bag system serve as a wall similar to a reinforced earth retaining wall.

The overflow depths (h_0 and h_1) on the upstream side and the centre of the crest were measured by using water gauges. To evaluate the displacement distribution of the downstream slope surface, a laser profiler with a servo motor control system was set in parallel with the downstream slope. For reference, a hydraulic test on a large-scale unreinforced embankment made using Kasama sand, 3.5 m high and 2.3 m wide with a downstream slope of 1V:1.8H, was conducted at a discharge unit quantity flow $q = 0.050$ m^3/s/m.

5.2.2. *Test conditions for GSET dam model*

Figure 16 shows the time history of discharge unit quantity flow in the overflow-induced collapse test on the GSET dam model. The flow rate was gradually increased from level 1 to level 3. Overflow water with a low flow rate went along the surface of the soil bag, and was basically in the state of nappe flow, although a small hydraulic jump occurred on each soil bag step.

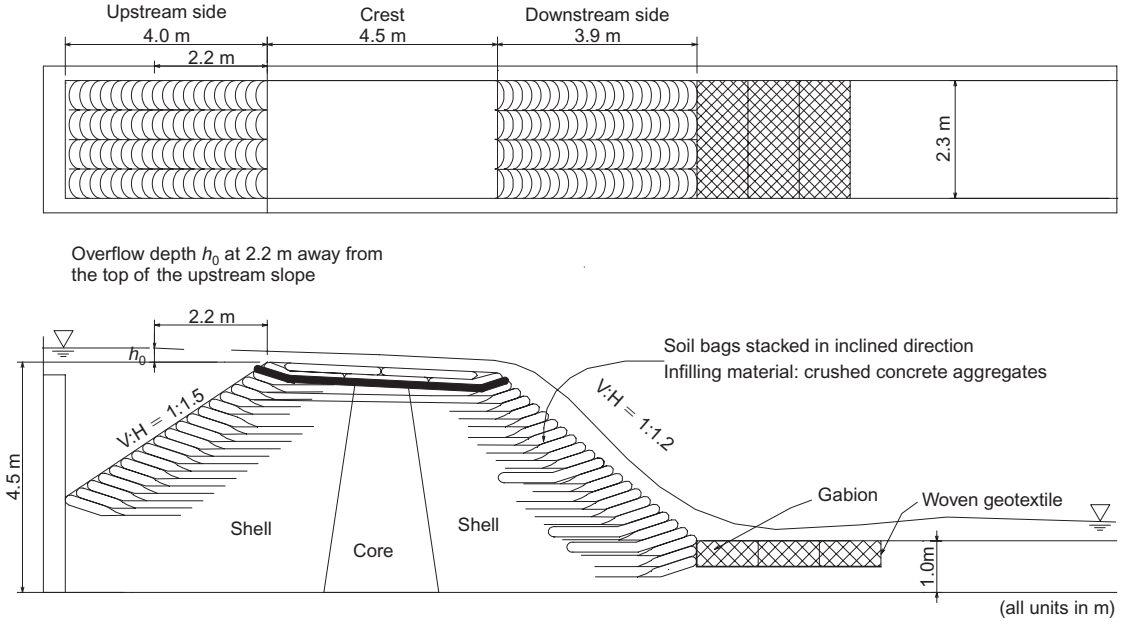

Figure 15. Test overview for large-scale breaching test (after Matsushima *et al.* 2007)

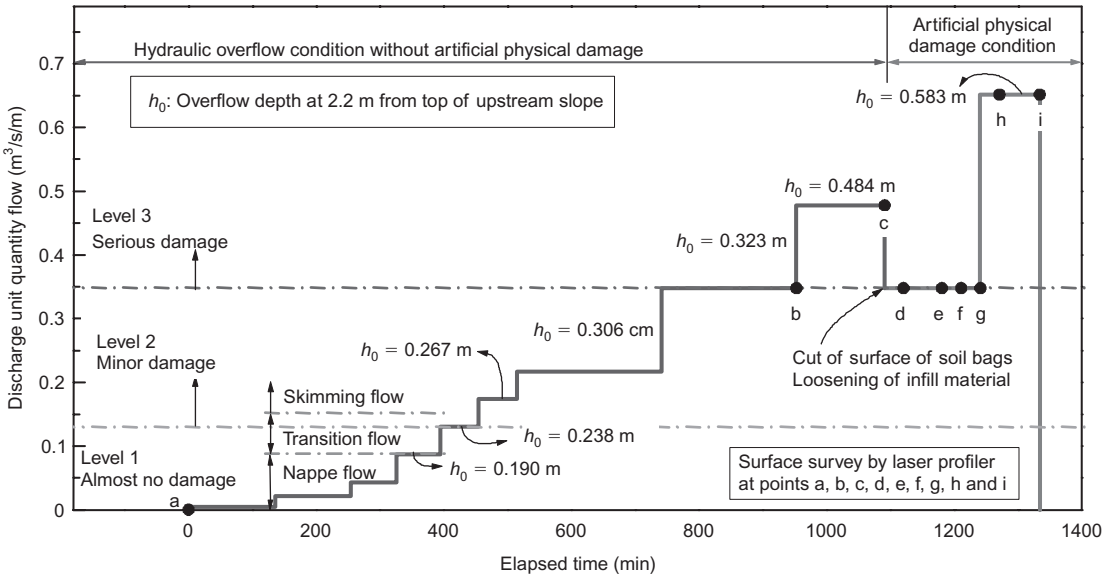

Figure 16. Time history of discharge unit quantity flow for test performed on GSET spillway model (after Matsushima *et al.* 2007)

Figure 16 also shows the ranges of flow level in which respective damage levels were observed during the test. The test consisted of the following two stages:

- Stage 1: without artificial physical damage to the soil bags;
- Stage 2: with artificial physical damage to the soil bags, by cutting the surface and loosening the backfill material in order to simulate damage by floating wood, chemical or ultraviolet degradation.

At the second stage, where the surface deformation by overflow became noticeable, at every step increase of overflow level at selected stages (denoted by letters a to i in Figure 16), surface surveys of the downstream slope were conducted by using the profiler.

5.2.3. *Overflow level 1 (little or no damage)*
When the overflow depth, h_0, was less than 0.238 m (i.e. S/d_c became 1.248–10.67, where S is step height and d_c is critical depth), a relatively steady flow in a staircase pattern was observed, owing to a high-energy dissipation caused by the soil bag steps. White water, which was actually richly aerated flow, was formed, and a small hydraulic jump impacted on each soil bag step (Figures 17a and 18). This stream regime was categorised into nappe or transition flow. This observation is consistent with the lower limit of S/d_c at which nappe flow is formed in stepped spillways: $S/d_c = 1.623$ at $\alpha = \tan^{-1}(1/1.2)$, according to Yasuda and Ohtsu (1999). Nappe flow, having nappe and air pockets, has no or little negative pressure at the corner of soil bags. Therefore suction of the backfill material from the slope behind the soil bags might not occur. Accordingly, no damage to the embankment, such as deformation, suction of backfill material or breakage of the soil bag, was observed.

5.2.4. *Overflow level 2 (minor or moderate damage)*
When the overflow depth, h_0, increased to between 0.238 m and 0.323 m (i.e. S/d_c became 0.649–1.248), a thick vein of head flow, separated from the top of the downstream slope, started forming, which impacted on a limited number of soil bags. As can be seen in Figure 19, a heavy flow started entraining air at some distance, after having leaped over several soil bag steps below the starting point (Figure 17b). This stream regime entraining

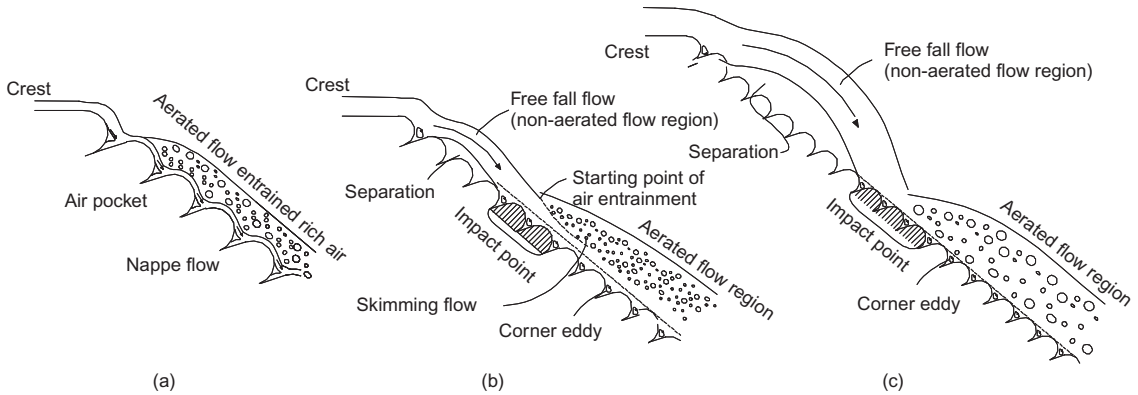

Figure 17. Schematic flow regimes in overflow levels: (a) level 1 (h_0 < 0.238 m); (b) level 2 (h_0 = 0.238–0.323 m); (c) level 3 (h_0 = 0.323–0.583 m)

Figure 18. Stream regime on downstream side at overflow level 1 at $q = 0.087$ m^3/s/m, $h_0 = 0.190$ m

Figure 19. Stream regime on downstream side at overflow level 2 at $q = 0.348$ m^3/s/m, $h_0 = 0.323$ m

air is basically classified as skimming flow, which is consistent with the upper limit of S/d_c for the formation of skimming flow in the case of a stepped spillway, $S/d_c = 1.126$ at $\alpha = \tan^{-1}(1/1.2)$. Skimming flow with a corner eddy creates suction at the corner. Therefore the damage observed on the slope at this stage included:

- suction of backfill materials from the slope behind the soil bags through the void area between the interfaces of adjacent soil bags;
- attrition of soil bag surfaces; and
- perforation of soil bags by sharp edges of the crushed concrete aggregates, induced by impact force.

Figure 20 shows the stacked backfill material that remained on the periphery of the void between the soil bags' interfaces after the test.

At the subsequent test stage, artificial physical damage was imposed on two soil bag columns at the centre, from 4 to 23 steps ($2 \times 20 = 40$ soil bags), by cutting the surface of geotextile soil bag and loosening the backfill material, as shown in Figure 21, during overflow testing for a total period of 150 min at a discharge rate of $q = 0.348$ m^3/s/m at the respective stages between damage operations.

As the damage expanded, some of the backfill materials were released. Thereafter, however, the bag sheet covered the upper fill materials again and adhered tightly to the whole surface of the embankment, so the overflow water did not erode the embankment's materials directly, resulting in no overall collapse of the dam.

5.2.5. *Overflow level 3 (serious damage)*

When the overflow depth, h_0, exceeded 0.323 m, a very thick vein of head flow with a free fall produced severe

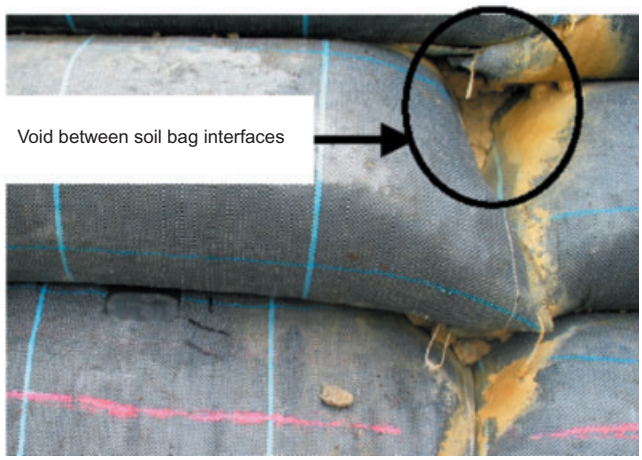

Figure 20. Evidence of sucked backfill material in cell zone behind stacked soil bags

Figure 21. Artificial physical damage: cutting surface of geotextile soil bag, and loosening backfill material

impact on a limited number of soil bags where the overflow water landed directly, causing the successive destruction of lower soil bags (Figures 17c and 22). Figure 23 presents the profile of the deformed downstream surface at stages b and c in Figure 16 (before artificial physical damage to the soil bags). It was found that a limited number of soil bags deformed severely, owing to impacts by over-fall of a very thick vein.

Figure 22 shows the profile of the deformed downstream surface after periods of 30 min and 90 min since the start of flow at a rate of $q = 0.652$ m^3/s/m, at stages h and i in Figure 16, after artificial physical damage to the soil bags. It was found that, after 90 min, the erosion had reached the foundation of the slope along the axis of waterfall formation, resulting in progressively more severe erosion. Figure 23 shows a trace of deep erosion that was formed by a waterfall. This erosion, which reached the foundation, is critical damage to the slope for the stability of the embankment. However, the rate of development of erosion with the reinforced slope was substantially slower than with the unreinforced slope, which collapsed at 5 min, as shown in Figure 24, at a much lower discharge of $q = 0.050$ m^3/s/m.

Even after this more severe erosion in the embankment, the settlement at the crest of the GSET dam was negligible, probably because of reinforcement effects. This high performance of the GSET dam shows that this technology can alleviate serious damage to the downstream slope caused by overflow of earth dams.

5.3. Summary of breaching tests

Based on these findings, it was demonstrated that GSET dam had great resistance to erosion and failure, and remained stable without complete collapse against large overflow. In addition, it is effective to place materials such as soil-cement and vegetation on the surface of the soil bags in order to ensure the durability of small earthfill dams.

It is suggested: (1) that a short slope with a gentle

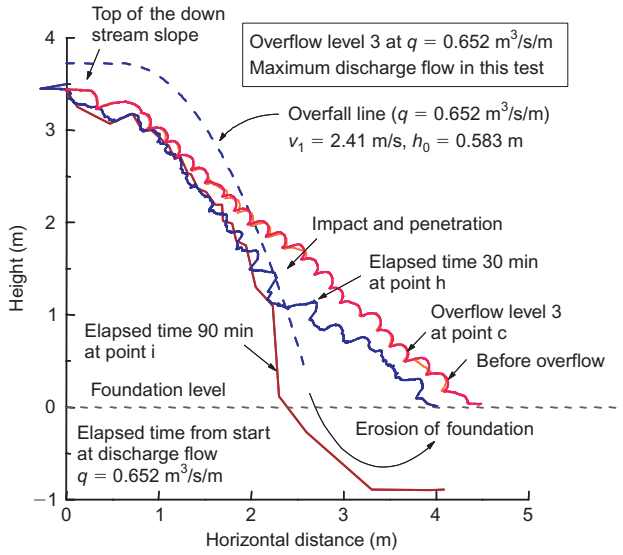

Figure 22. Distributions of horizontal displacement on downstream slope surface (after Mohri *et al.* 2007)

Figure 23. Erosion trace like the formation of a waterfall basin after final overtopping

Figure 24. Erosion trace on unreinforced soil slope after 5 min at $q = 0.050$ m^3/s/m

gradient should be arranged from the top corner to the impact point at the upper part of the downstream slope; and (2) that the surface of the soil bags at the impact point should be reinforced to provide sufficient resistance against penetration force.

The development rate of erosion was significantly slower than with the unreinforced slope, and settlement of the crest was negligible. Therefore total collapse might not occur, even during a very strong flood. It is concluded that the GSET dam is effective technology to prevent collapse of the downstream slope by overflow of earthfill dams.

6. COMPRESSION STRENGTH OF STACKED SOIL BAGS

6.1. General

The use of geosynthetics in closed form, such as soil bags, is also becoming attractive (e.g. Tatsuoka *et al*. 1997; Matsuoka *et al*. 2001; Lohani *et al*. 2004). Stacking soil bags to form a structure is a practical and cost-effective solution when construction space is limited, and also when rapid construction is required.

It is important to ensure that the stacked soil bags used to stabilise an old earthfill dam are high strength in order to increase the stability of the dam dyke itself.

With the aim of using of a soil bag pile as a structural component of a permanent civil engineering structure supporting external load, the strength and deformation characteristics of a sand bag pile subjected to vertical compressive force were evaluated experimentally. The effects of the following factors were studied.

- Compaction of backfill: It was examined whether the backfill placed in the soil bag should be compacted to ensure a high performance.
- Material type of soil bag: Two different types of geosynthetic, a stronger one and a weaker one, were used.
- Backfill type: In addition to three types of natural soil, a recycled product of crushed concrete aggregate was used.
- Vertical preloading: The initial stiffness at relatively small compression of virgin soil bags is very low. It was examined whether this inherent drawback of soil bags can be alleviated by applying appropriate vertical compressive preload.

6.1.1. *Soil bag materials*

Polyethylene (PE) and polypropylene (PP) geosynthetics were used in these tests as soil bag materials:

- Polyethylene sheet (PE): a relatively weak material with a tensile rupture strength of 3.75 kN/m. This is used mostly in temporary works.
- Polypropylene sheet (PP): this is a relatively strong material with a tensile rupture strength of 14.5 kN/m, but it needs to be protected from ultraviolet light.

Tensile loading tests were conducted on specimens 100 mm long and 50 mm wide, at a strain rate of 1%/min, as shown in Figure 25. It may be seen that the PP sheet is considerably stronger and stiffer, by a factor of about four, than the PE sheet, while the tensile strain at peak is nearly the same.

6.1.2. *Backfill materials and test*

Recycled concrete aggregate has mainly been used as a material for filling soil bags, but considering the cost-effective use of locally excavated material, sands mixed with different proportions of clay fraction were also tested as backfills. The materials used were:

- recycled electric pole concrete aggregate, REPA, with $D_{max} = 37.5$ mm (material A);
- Toyoura sand (material B);
- Hokota sand (material C);
- FC35 (material D, a mixture of Hokota sand and Kanazawa clay in 7:3 proportion by mass); and
- FC50 (material E, a mixture of Hokota sand and Kanazawa clay in 1:1 proportion by mass).

Figure 26 shows the grain size distribution curves of the backfill materials. Only REPA was used as backfill of the

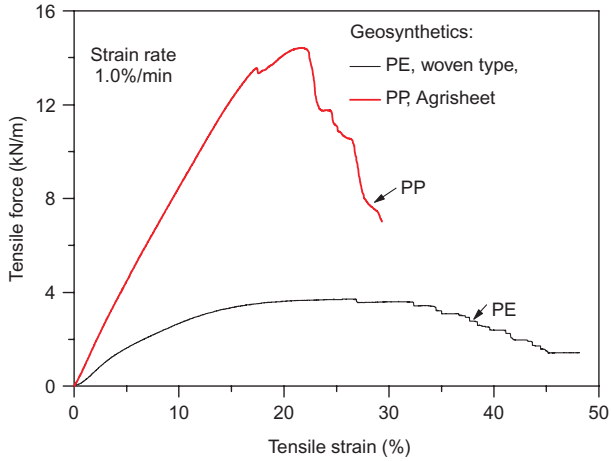

Figure 25. Tensile force–strain relation for tensile test on PE and PP woven geosynthetic used as soil bag material (after Lohani *et al.* 2006)

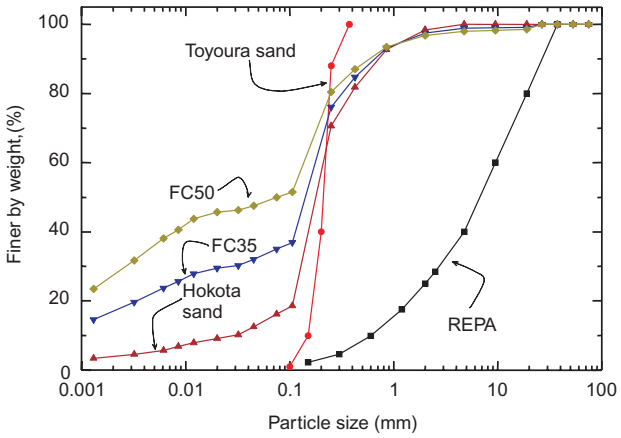

Figure 26. Particle size distribution curves of backfill materials (after Lohani *et al.* 2006)

specimens for the series L vertical compression tests in the laboratory.

Two main methods were used to prepare the soil bags:

- Series L: The effects of backfill compaction and the soil bag material on the strength and deformation characteristics of a stacked sand bag pile were evaluated. The total mass of a filled bag was 195 N per bag (REPA), which was about 50% of its full volume. The filled bags were placed under a vibrating rammer of mass 1.70 kN.
- Series F: The compression behaviour of soil bags made of four different types of backfill, compacted in a manner similar to those adopted in the field, was evaluated by applying two heavy (3.50 kN) vibratory compactor passes. Soil bags made of PP were filled with 390 N of backfill, at nearly 100% of the capacity of each soil bag for the standard Proctor compaction energy level. Four different types of backfill material (materials A, C, D and E) were packed in the PP geosynthetic bags.

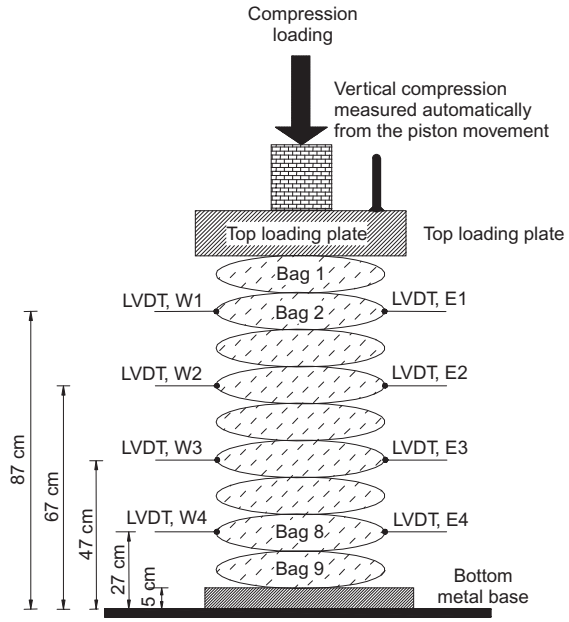

Figure 27. Experimental set-up with measurements for stacked soil bags for vertical compression tests, series F (after Lohani *et al.* 2006)

A series of unconfined compression tests was conducted on the stacks of geosynthetic soil bags filled with various geomaterials. A constant strain rate of loading of 1.08 mm/min was maintained in all the tests. Table 3 lists the soil bag specimens in these compression tests, and Figure 27 shows the test device and experimental set-up of soil bags in test series F (Table 3).

6.2. Effect of initial compaction of soil bags

Figures 28a, 28b and 28c show the relationships between the average axial compressive stress, $\sigma_{v,ave}$, and the average axial strain, $\varepsilon_{v,ave}$, of soil bag piles from series L tests performed at an average axial strain rate of 0.35%/min. The results from continuous monotonic loading tests (L1, L2 and L7) are presented in Figure 28a.

Table 3. Tests on soil bag specimens (modified from Lohani *et al.* 2006)

(a) Series L compression tests

Test case	No. of bags	Bag material	Average initial dimensions of soil bag (mm)			Average dry unit weight (kN/m^3)[a]	H/W ratio of soil bag pile	Compaction
			Length	Width	Height			
L1	4	PE	491	386	245	15.4	0.62	Yes
L2	4	PE	399	379	312	15.0	0.82	No
L3	4	PE	402	379	303	15.4	0.80	No
L4	4	PE	404	378	303	15.4	0.80	No
L5	4	PE	488	405	247	15.1	0.61	Yes
L6	4	PE	476	411	243	15.4	0.59	Yes
L7	4	PP	487	417	235	15.3	0.56	Yes
L8	4	PP	486	427	232	15.2	0.54	Yes
L9	4	PP	486	433	233	14.9	0.54	Yes

(b) Series F compression tests

Case no.	Average initial dimensions of soil bags (mm)			Water content (%)	Average dry unit weight (kN/m^3)[a]	Backfill material	H/W ratio of soil bag pile
	Length	Width	Height				
F1	543	400	930	9.6	16.1	REPA	2.33
F2	505	400	972	16.3	15.6	Hokota	2.43
F3	553	414	961	18.7	13.7	FC35	2.32
F4	560	420	920	19.4	13.8	FC50	2.19

[a]Average dry unit weight = total backfill weight/volume (the volume was calculated from the approximate dimensions of the soil bag pile). Series L: backfill = REPA; series F: bag material = PP, no. of bags = 9.

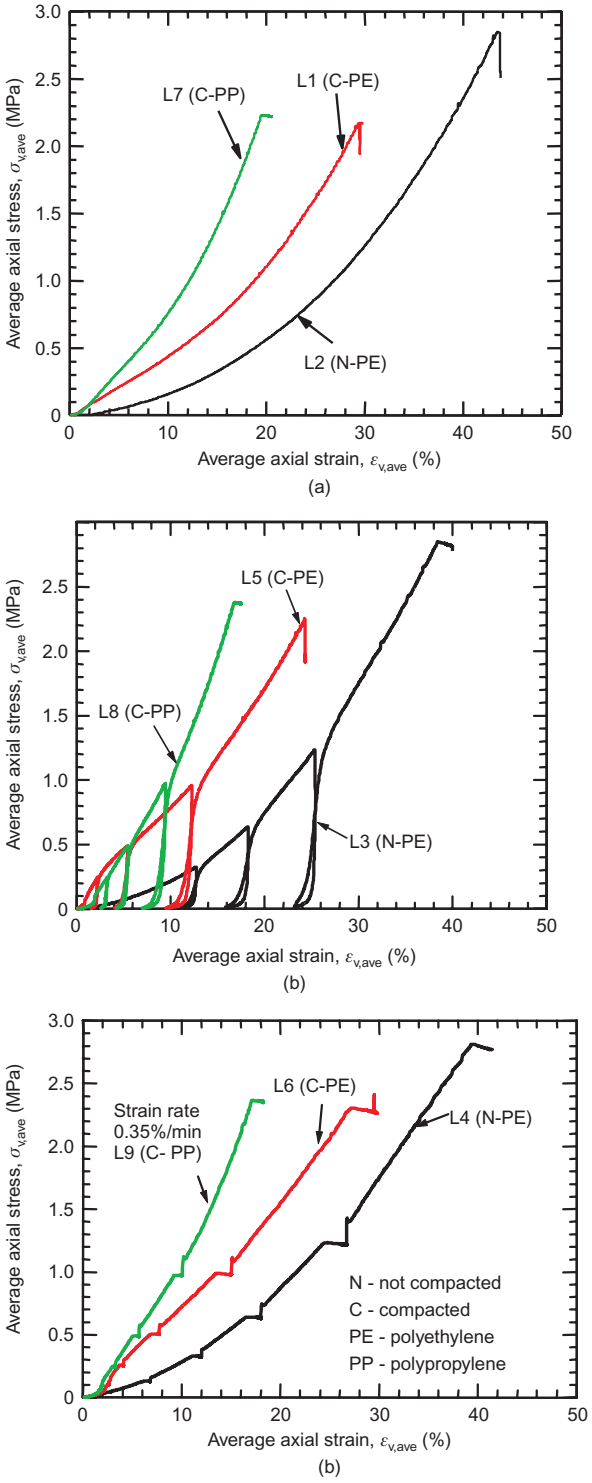

Figure 28. Average stress–strain relations from vertical compression tests on stacked soil bags, showing effect of initial compaction, and material used for bags (after Lohani *et al.* 2006): (a) compaction effect; (b) preloading effect; (c) creep effect

The effects of initial backfill compaction were evaluated by using soil bags made of PE. The initial stiffness at small strains of the respective compacted specimen (denoted by C) is noticeably higher than that of the corresponding non-compacted one (denoted by N).

As can be seen from Figure 28a, the initial stiffness against relatively small compressive deformation of a soil bag pile with uncompacted backfill is very low. It is also true that the $\sigma_{v,ave}$ value increases at a very low rate for the initial stage of loading, particularly when the backfill is not initially compacted. Furthermore, a large axial strain is necessary to reach the ultimate compressive strength. These features are among the largest potential problems with soil bags when used as part of a soil structure allowing a limited amount of deformation.

6.3. Effect of geosynthetics used to prepare soil bags

The effects of geosynthetic type (PE and PP) on the stress–strain behaviour of soil bag are readily seen by comparing the results from test pairs L1 and L7, L5 and L8, and L6 and L9. That is, the stiffness of the soil bag increases with an increase in the stiffness of the bag material. However, when the backfill is initially compacted, the difference in the stiffness at small strains becomes smaller and insignificant. This means that, to obtain high initial stiffness of soil bags at smaller strains, a high initial compaction of the backfill is more important than using a soil bag material with a high stiffness. On the other hand, Figure 29 compares creep strains in the three tests described in Figure 28c. It is understood by comparing the results from tests L6 (PE) and L9 (PP) in Figures 28c and 29 that the creep strain also decreases with an increase in the stiffness of the soil bag material, which becomes more obvious with an increase in the stress level.

6.4. Effectiveness of preloading

In Figure 28b, when compared at the same axial stress, the tangent stiffness during reloading is substantially higher than that during primary loading. This trend is more obvious at small stress levels. These results indicate that the most effective way to increase the stiffness of soil bags is to develop large residual tensile force in the soil bags by applying relevant preload.

6.5. Effect of backfill materials used in soil bags

Figure 30 shows the average stress–strain response of the stacked soil bags in the series F tests. Unloading to near zero stress and then reloading were performed many times

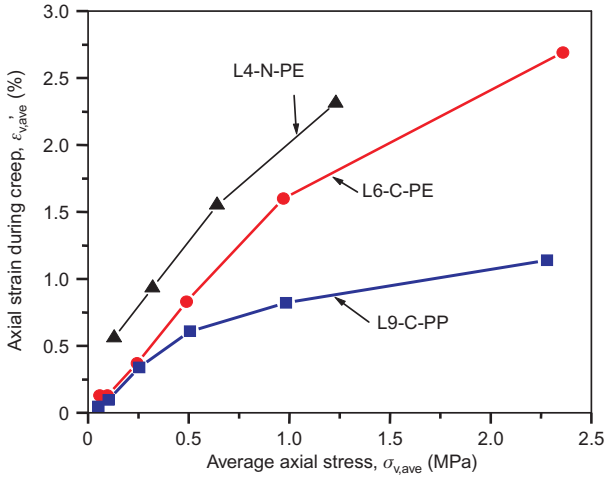

Figure 29. Effect of compaction and material used for soil bag preparation in series L tests (after Lohani *et al.* 2006)

to evaluate the effectiveness of preloading. In the tests, very similar loads were repeatedly applied on the stacked soil bags by changing the backfill material. The general trend is that the REPA material, which is a well-graded gravel with a higher angle of internal friction, is better than the finer soils (Hokota sand, FC35 and FC50).

Although the backfill material with the largest percentage of fines was expected to show the weakest behaviour, the tests with FC50 infill differed slightly. The results may be summarised as follows:

- Both the strength and the stiffness of soil bags are improved by using stronger geosynthetic bags.
- Well-graded REPA aggregate is better suited as a backfill material for soil bags than those containing a large proportion of fines.
- The soil bag system shows a clear increase in stiffness during the reloading phase.
- While the initial response is not so encouraging, the stronger stress–strain behaviour and negligible creep strain during the reloading phase confirm that soil bags can be used cost-effectively in civil engineering works when sufficient preload is applied.

7. LATERAL SHEAR TESTS ON STACKED SOIL BAGS

7.1. General

Regarding the lateral deformation of a reinforced-soil structure, although it is assumed to be a rigid body in many design codes, Tatsuoka *et al*. (1998) demonstrated that the simple shear deformation of reinforced-soil retaining wall models was not negligible in reduced-scale shaking-table tests, and Bathurst and Hatami (1998) showed the same behaviour for the reinforced zone by FLAC model analysis. During seismic events, stacked soil bag systems may be subjected to lateral shear loading, in which the global direction of compressive load is greatly inclined from the vertical direction. In such a case, the strength and deformation characteristics, which are essential for a reliable seismic design, are not known. The strength under lateral shear is likely to be very different from that under vertical compression, owing to the highly anisotropic structure of stacked soil bags.

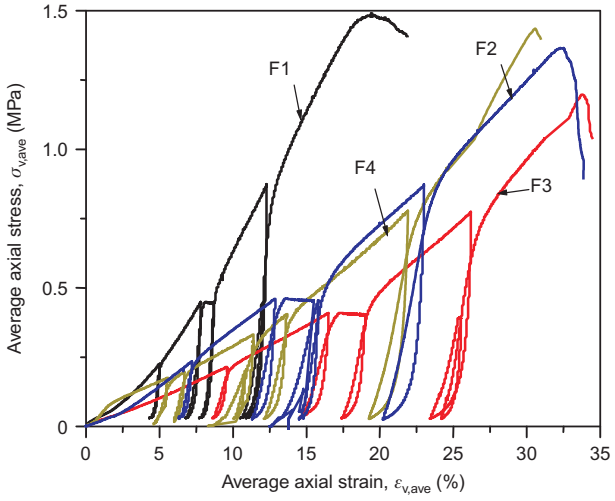

Figure 30. Average axial stress–strain relation for series F test specimens with various backfill materials (after Lohani *et al.* 2006)

Several researchers have studied the sliding resistance at the bag-to-bag interfaces, typically in terms of the interface friction (e.g. Matsuoka *et al*. 2003; Krahn *et al*. 2007). In reality, however, the failure of stacked soil bags by lateral shear loading is controlled not only by slippage along the bag-to-bag interface, but also by excessive deformation of the soil bags owing to failure of the backfill or rupture failure of the soil bag sheet. It is necessary therefore to understand these two failure mechanisms of multi-layered soil bags.

In view of the above, a series of full-scale lateral shear tests on a stacked soil bag system was conducted by Matsushima *et al.* (2008).

The first objective is to find an effective practical method to improve the stability of multi-layered soil bags subjected to lateral shear loading. The second objective is to understand which of the two mechanisms (slippage along the bag-to-bag interfaces or shear deformation) applies for given multi-layered soil bags under given loading condition.

7.2. Test method

To evaluate the shear strength and stiffness of a soil bag system accurately, a single stack of full-scale soil bags was used, as shown in Figure 31. Also, to increase the shear strength of the soil bag system, the bags were arranged with an inclined interface between vertically adjacent bags. The angle, δ, of the direction of the interface relative to the horizontal was set at 18°, as well as at 0° for reference. To investigate the failure mechanism of the soil bag system, and in particular to examine whether failure is caused by shear deformation of bags or by slippage at the interface between vertically adjacent soil bags, lateral displacements of soil bags were measured with a set of pulley-type LVDTs (S1 to S6 and S).

The respective full-scale soil bags were each filled with 1.20 kN of air-dried Toyoura sand. The geotextile used as the soil bag sheet was a woven polypropylene. To produce each specimen, the bottom soil bag, among in total three soil bags for a single specimen, was first compacted by using a 1.70 kN vibratory compactor. The soil bag for the next layer was placed on the compacted bottom soil bag and compacted in the same way. The last soil bag was then placed on the former layered soil bags and compacted. All the specimens had been compacted in the same way, for a compaction duration of 5 min using the 1.70 kN vibratory compactor.

7.3. Shear behaviour of stacked soil bags

Figure 32 shows the relationships between the stress ratio, τ_{vh}/σ_v, the shear displacement, s, and the vertical displacement, d, both at the top of the specimen and relative to the bottom, from six tests on a single stack of three soil bags filled with Toyoura sand. These figures reveal the following trends. Both the peak τ_{vh}/σ_v value and the pre-peak

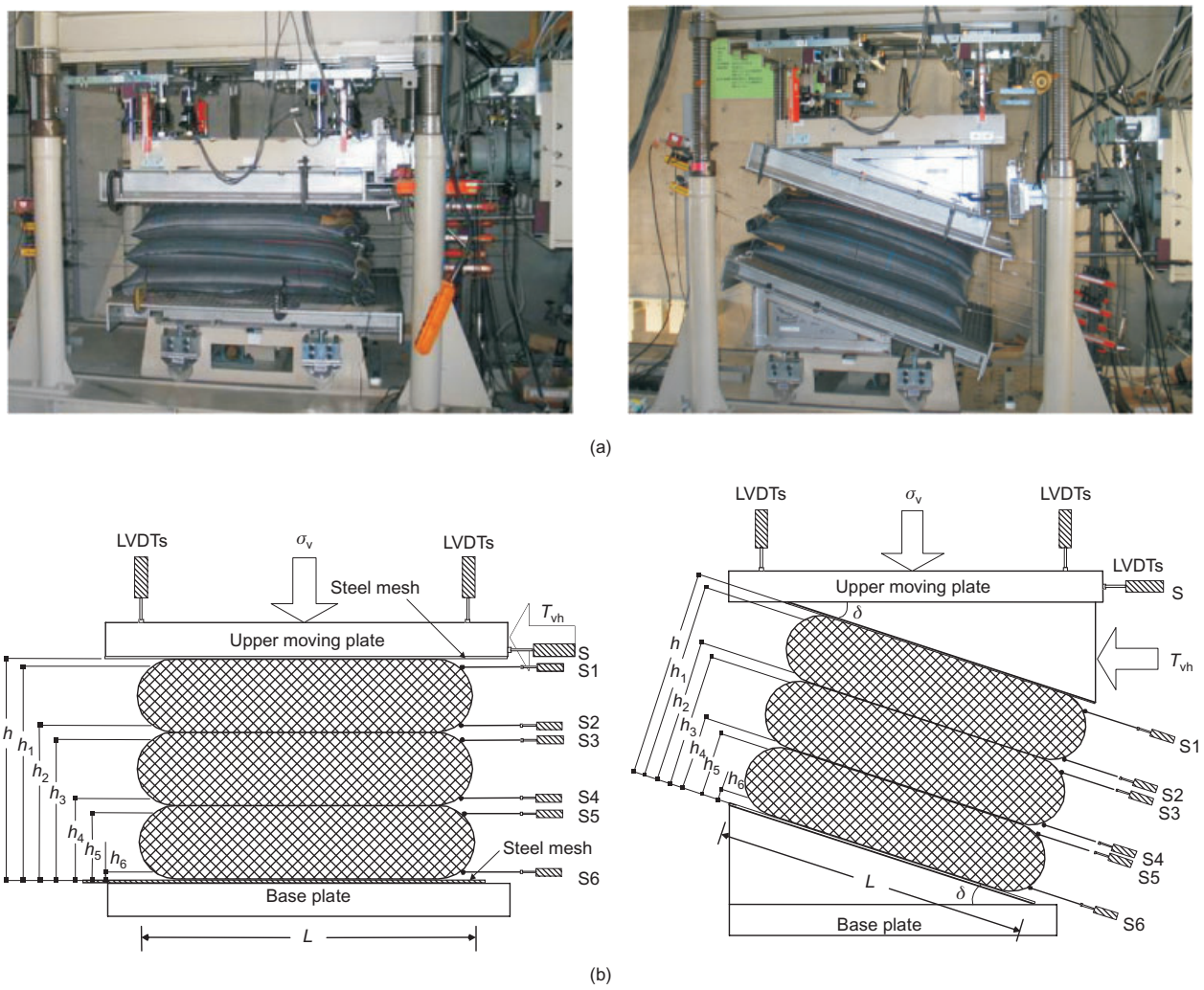

Figure 31. Schematic diagram of soil bag shear test apparatus with LVDTs to measure lateral displacements of bags, stacked horizontally ($\delta = 0°$) and inclined ($\delta = 18°$) (after Matsushima *et al.* 2008): (a) test apparatus with a specimen; (b) schematic diagram

stiffness increased significantly, by about 1.6–2.0 times, upon changing the angle δ from 0° to 18°. The volumetric change also changed significantly, from contractive to dilative.

This result indicates that soil bags stacked on an inclined slope can exhibit an interlocking mechanism and a significantly larger resistance when shear-loaded laterally.

Figure 33 shows the vertical distribution of lateral displacement at the front side face of the soil bags observed at different lateral shear displacements ($\delta = 18°$, Toyoura sand at $\sigma_v = 30$ kPa). It can be seen that, at this low σ_v value, noticeable relative lateral shear displacements take place between the top and middle soil bags (i.e. between S2 and S3). This result indicates that slippage took place along the bag-to-bag interface, which increased with an increase in the lateral shear displacement at the top loading platen. On the other hand, the relative shear displacements between S1 and S2, between S3 and S4 and between S5 and S6, which correspond to the shear deformations of the respective soil bags, remained quite small, and did not increase with an increase in the lateral shear displacement at the top loading platen. These results indicate that the failure mode in this case is slippage along the bag-to-bag interface, as shown in Figure 34a.

At high σ_v (i.e. 300 kPa), the peak τ_{vh}/σ_v value was controlled by shear failure in the sand inside the soil bags, as illustrated in Figure 33b. That is that the slippage along the interfaces between two vertically adjacent soil bags is much smaller than the shear deformations in the respective soil bags. This is because the increase in the sliding resistance at the bag-to-bag interfaces with the increase in σ_v was greater than that of the shear strength of the backfill. Therefore, which failure mode, slippage (Figure 34a) or simple shear (Figure 34b), actually takes place depends on the relative magnitude of these two types of strength.

These test results indicate that a soil bag system becomes much more stable simply by being placed inclined so that the direction of the bedding planes of the soil bags becomes normal to the principal direction of the applied compressive load. Moreover, to maximise the shear strength it is important to prevent slippage at the interface between adjacent soil bags, particularly when the applied normal stress is low.

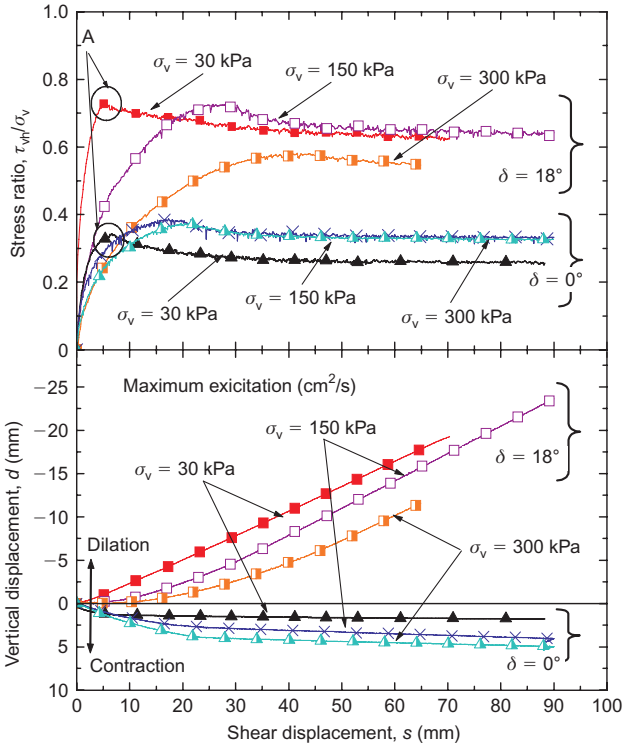

Figure 32. Results from shear tests on sand bags of Toyoura sand stacked horizontally and inclined: top, shear stress ratio; bottom, average vertical displacement (after Matsushima *et al.* 2008).

8. SHAKING TESTS OF GSET DAM AND ANALYSIS

In order to evaluate the ultimate performance and stability under strong earthquake, analytical prediction of the permanent displacement was performed on the newly proposed high-performance earthfill dam with GSET. Moreover, shaking-table tests were performed on a model of the dam (Arangelovski *et al.* 2006; Matsushima *et al.* 2006a).

8.1. Test results

The shaking-table tests were performed on a three-directional shaking table at the National Institute for Rural Engineering. According to the projected experimental programme for shaking-table tests, the performance of two types of earthfill dam was investigated: a horizontally stacked model and an inclined stacked model with GSET, using the same size as the full-scale soil bag. A three-directional shaking table with dimensions 6 m × 4 m and maximum load capacity of 500 kN was used.

The model earthfill dam had a height of 2200 mm, crest width of 1700 mm, downstream slope of 1V:1H and upstream slope of 1V:1.5 H, as shown in Figure 35. The body of the dam was constructed with silty sand (Kasama sand) with density of $D_r \approx 90\%$. The woven soil bags made of polypropylene sheet were filled with recycled crushed concrete aggregate REPA.

The input acceleration had a sinusoidal shape with frequency $f = 3.8$ Hz and five levels of intensity a_{max}, as shown in Figure 36: 3 m/s², 5 m/s², 7 m/s², 10 m/s² and 12 m/s².

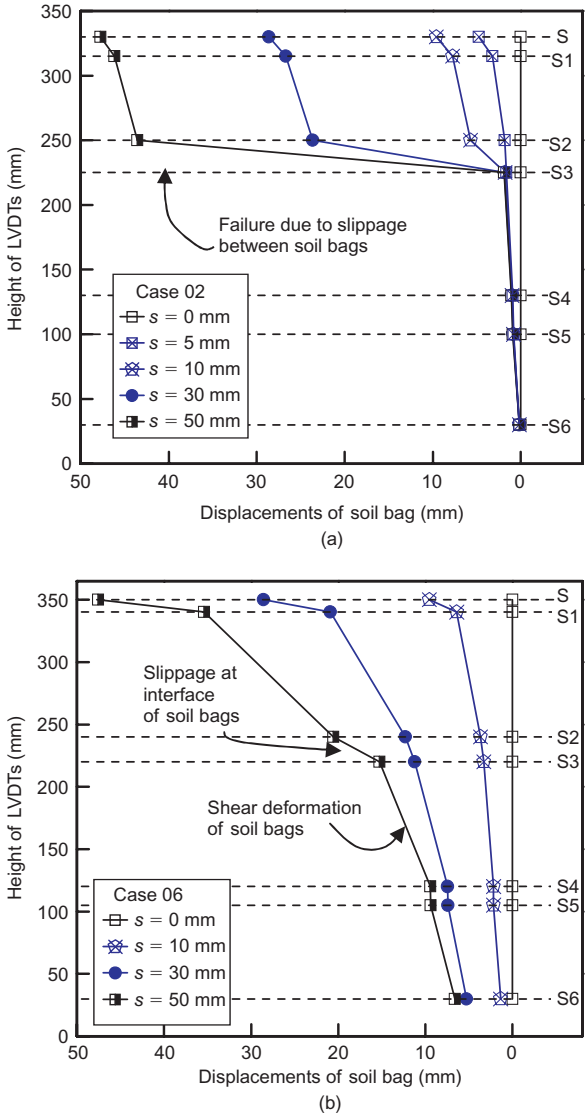

Figure 33. Distribution of lateral displacement at front face of soil bags filled with Toyoura sand stacked inclined in a shear test (after Matsushima *et al.* 2008): (a) $\sigma_v = 30$ kPa; (b) $\sigma_v = 300$ kPa

The experimental results can be summarised as follows. Lateral displacements of the soil bag surface along the slope were increased with shaking. On the downstream slope, when the intensity of input acceleration was low ($a_{max} = 3$ m/s²), the stacked soil bags behaved like a rigid body without being separated from the main body of the dyke. At this stage, the difference in lateral behaviour between the two models having horizontal and inclined soil bags (cases H and I) was not significant, as shown in Figure 37. Figure 38 shows residual settlements of the crest observed after each excitation for the two models. In the horizontal model, the crest settlement became 25 mm at 3 m/s² excitation and increased to 210 mm settlement at 5 m/s², which was a settlement ratio against the model height of 9%. At input acceleration $a_{max} = 7$ m/s², some slippage took place between adjacent soil bags at the middle of the slope, and the crest settlement became 450 mm, which was 18% of the initial model height.

The other model with inclined soil bags was much more

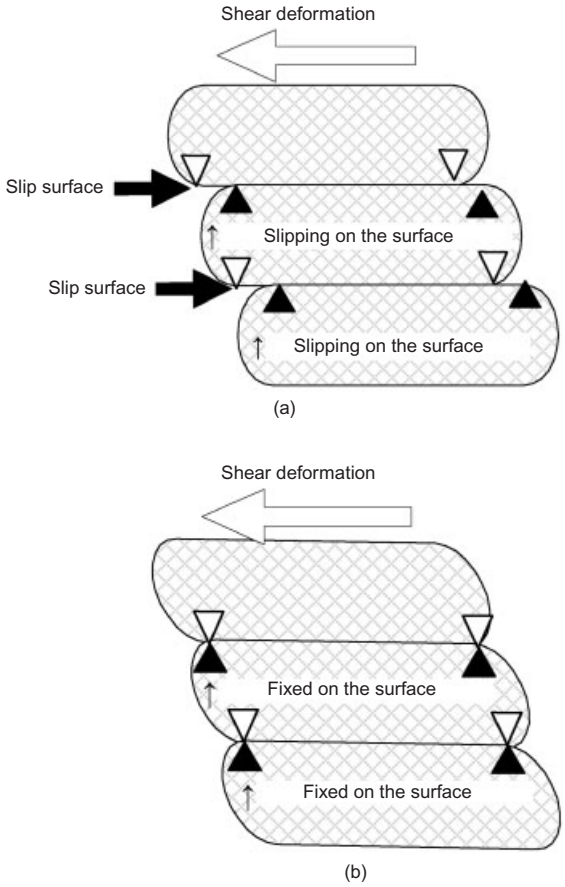

Figure 34. Two failure modes of multi-layered soil bags subjected to lateral shear loading: (a) slippage failure at interface of bags (direct shear); (b) shear failure in backfill (simple shear).

stable. The crest settlement was negligible at 3 m/s^2 excitation, and reached only 23 mm at 5 m/s^2 excitation. It caused 100 mm settlement at 7 m/s^2, which was very small: only 25% of the settlement of the horizontal model. For stronger shaking amplitudes, $a_{max} = 10$ m/s^2, the dam

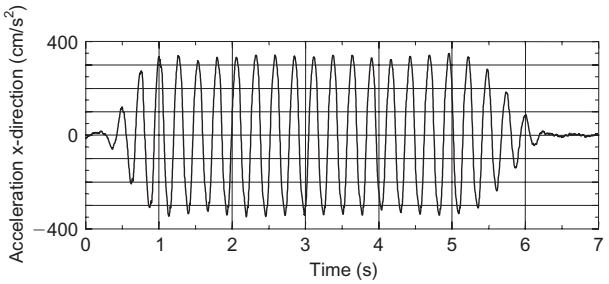

Figure 36. Sinusoidal input acceleration: $a_{max} = 348.718$ cm/s^2; $a_{min} = -348.718$ cm/s^2; frequency $f = 3.48718$ m/s^2, -3.48718 m/s^2

exhibited a large vertical deformation of 304 mm, and the surface of the soil bag deformed into a round shape, but there was no slippage between stacked soil bags, as for the horizontal model.

The crest of the dam subsided with large vertical displacement only during strong shaking. After the experiment the dam was carefully sliced longitudinally in order to investigate the inner mode of deformation. Figure 39 shows the two types of failure mode for each test model. With the horizontal model (case H, Figures 39a and c), the shear failure planes (i.e. failure zone or failure band) for the embankment consist of two parts: a sliding surface just behind the soil bag wall, and the interface plane between the stacked bags. With the inclined model (case I, Figures 39b and d), the failure planes consist of shallow and deep circular sliding surfaces inside the embankment, which pass through a separation at the bottom of the soil bag wall.

These experiments showed that the GSET structure with the inclined stacking method has a high seismic stability (i.e. reduced ultimate deformation of the slope and settlement of the crest) without total failure of the embankment. In this case, the soil bag wall and the zone immediately behind in the embankment were very stable. Therefore, the failure surfaces appeared only in the deep zone in the dam, which resulted in a higher stability.

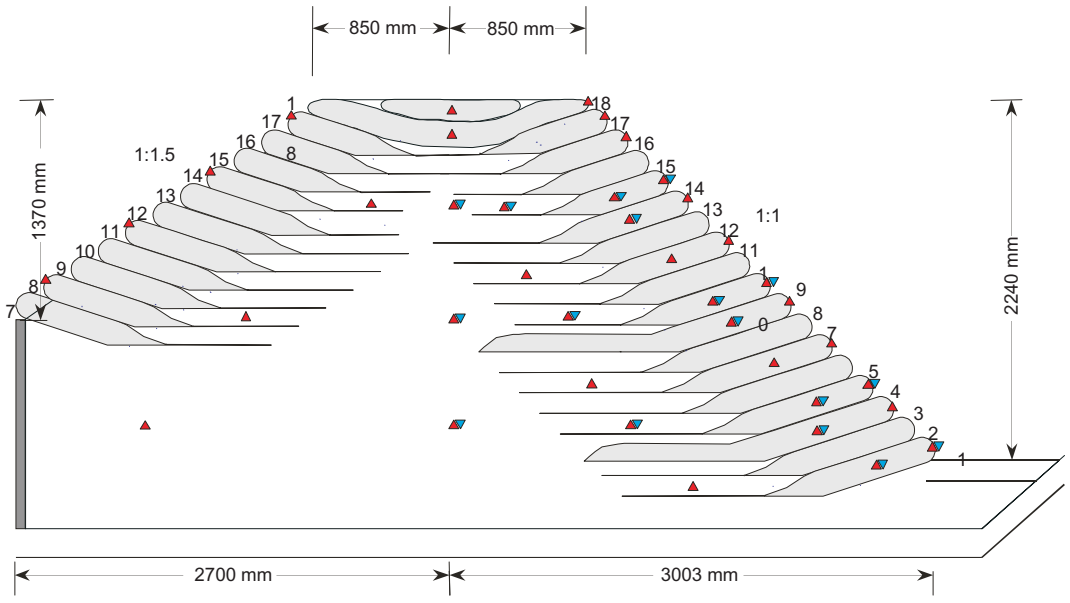

Figure 35. Cross-section of GSET reinforced earth dam (inclined model)

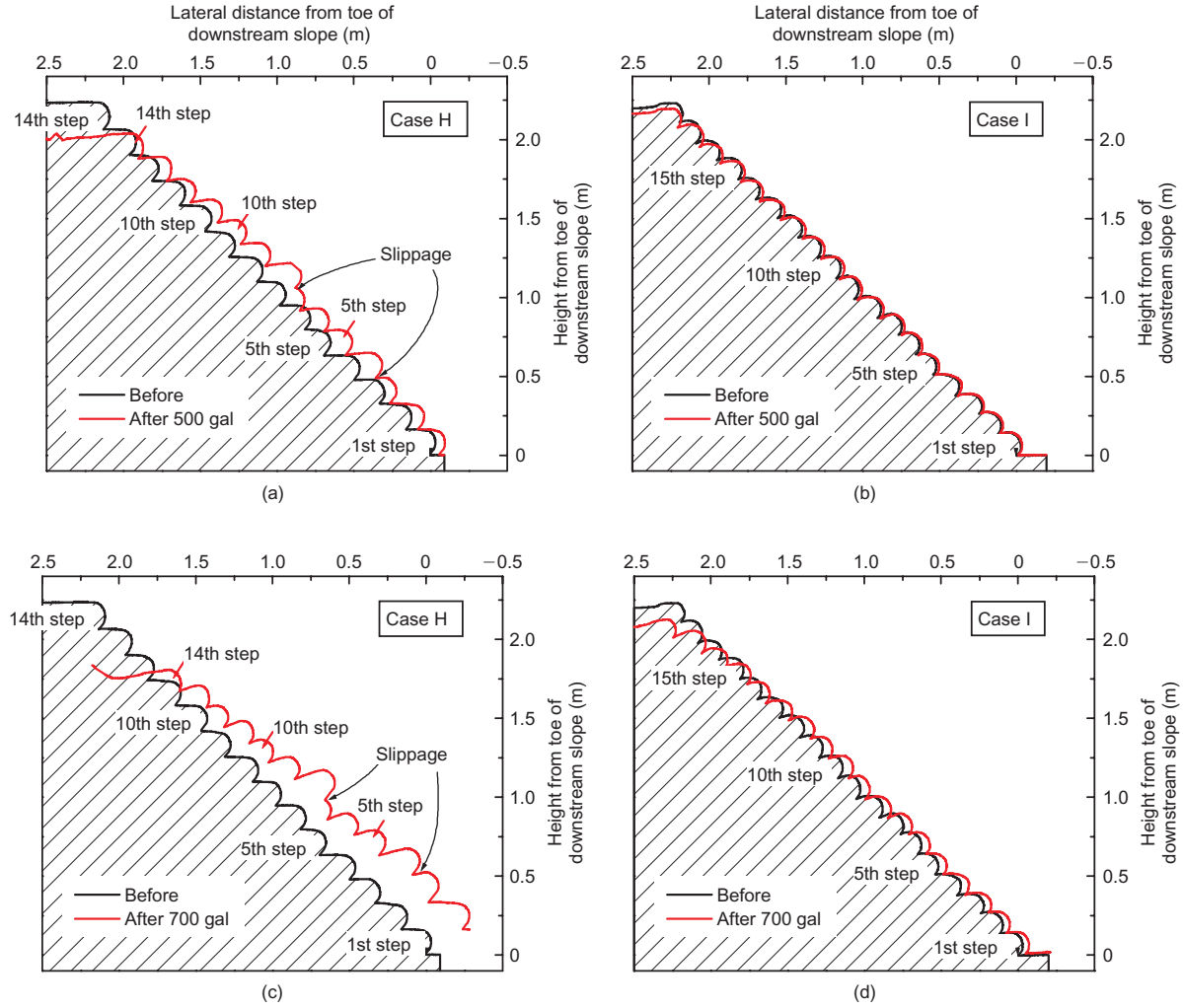

Figure 37. Lateral displacement of soil bag surface along slope, horizontally stacked model (case H) and inclined stacked model (case I) at each excitation level: (a) 5 m/s^2, horizontal stacking; (b) 5 m/s^2, inclined stacking; (c) 7 m/s^2, horizontal stacking; (d) 7 m/s^2, inclined stacking

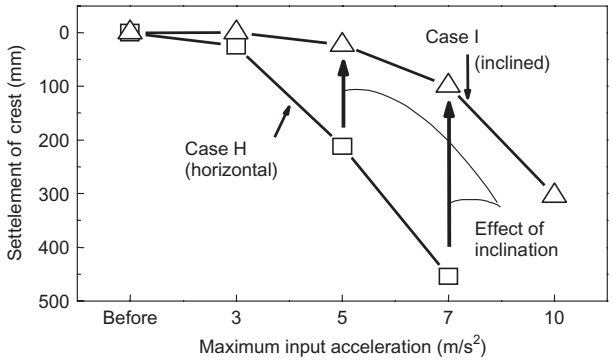

Figure 38. Settlement of crest for GSET dam models (horizontal and inclined) at each excitation level

8.2. Analysis of GSET dam

8.2.1. *Dynamic solution method*

Dynamic response analysis, combined with the generalised return-mapping algorithm, was applied to the integration algorithms of the elasto-plastic constitutive relations, including the effect of the shear band. The explicit dynamic response analysis was applied to the solution of the embankment dam. The perfectly plastic, isotropic hardening-softening and kinematic hardening models were employed.

The solution of the dynamic equation of motion can be obtained by

$$M_{\mathrm{D}}a + Cv + P - P^{\mathrm{init}} = F \tag{1}$$

where M_{D} is the diagonalised mass matrix, C is the damping matrix, v is the velocity vector, a is the acceleration vector, P is the internal force vector, P^{init} is the nodal forces due to initial stresses, and F is the external force vector.

Applying the central difference method to Equation 1 and replacing the damping by the relation

$$C = \alpha_{\mathrm{damp}} M_{\mathrm{D}} \tag{2}$$

the following relaxation equation can be derived.

$$q_{n+1} = \frac{1}{1 + 0.5\alpha_{\mathrm{damp}}\Delta t} \times \left[\frac{\Delta t^2}{M_{\mathrm{D}}}(F - P + P^{\mathrm{init}})^t + 2q_n - (1 - 0.5\Delta t)q_{n-1}\right] \tag{3}$$

Here q_n is the displacement vector at time n, Δt is the time increment, and α_{damp} is the damping ratio.

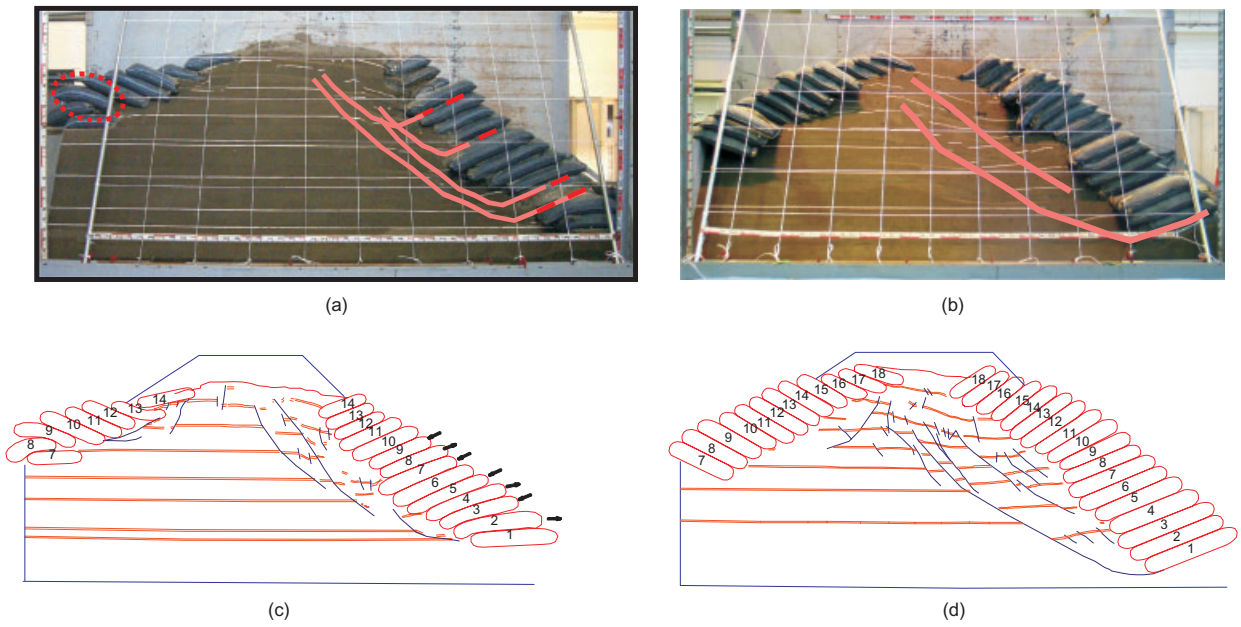

Figure 39. Failure mode of GSET dam models (horizontal and inclined) after stronger excitation: (a) horizontal stacking, after 7 m/s^2 (case H); (b) inclined stacking, after 10 m/s^2 (case I); (c) horizontal stacking (case H); (d) inclined stacking (case I)

8.2.2 *Constitutive model for plasticity*

A simplified and generalised version of the mesh-size-dependent softening modulus method was used in this study. A material model for a real material was used, with the following features: non-linear pre-peak, pressure sensitivity of the deformation and strength characteristics of sand, non-associated flow characteristics, post-peak strain-softening, and strain-localisation into a shear band with a specific width.

The yield function, f, and the plastic potential function, Φ, are given by

$$f = \alpha I_1 + \frac{\overline{\sigma}}{g(\theta_L)} = 0 \tag{4}$$

$$\Phi = \alpha' I_1 + \overline{\sigma} = 0 \tag{5}$$

where

$$\alpha = \frac{2\sin\phi}{\sqrt{3}(3-\sin\phi)} \qquad \alpha' = \frac{2\sin\psi}{\sqrt{3}(3-\sin\psi)} \tag{6}$$

where I_1 is the first invariant (positive in tension) of deviatoric stresses, and $\overline{\sigma}$ is the second invariant of deviatoric stress. With the Mohr–Coulomb model, $g(\theta_L)$ takes the form

$$g(\theta_L) = \frac{3-\sin\phi}{2\sqrt{3}\cos\theta_L - 2\sin\theta_L\sin\phi} \tag{7}$$

where ϕ is the mobilised friction angle and θ_L is the Lode angle. The frictional hardening–softening functions expressed as follows were used:

$$\alpha(\kappa) = \left(\frac{2\sqrt{\kappa\varepsilon_f}}{\kappa+\varepsilon_f}\right)^m \alpha_p \quad (\kappa \leqslant \varepsilon_f): \text{ hardening-regime} \tag{8}$$

where m, ε_f and ε_r are material constants, and α_p and α_r are the values of α at the peak and residual states. The residual friction angle (ϕ_r) and Poisson's ratio (ν) were chosen based on data from the triaxial tests on the sand used in the model tests. The peak friction angle (ϕ_P) was estimated from empirical relations based on the plane-strain compression test on dense sand. ψ is the dilatancy angle. The introduction of shear banding in the numerical analysis was achieved by introducing a strain localisation parameter s in the following additive decomposition of total strain increment:

$$d\varepsilon_{ij} = d\varepsilon^e_{ij} + s\,d\varepsilon^p_{ij}, \quad s = F_b/F_e \tag{9}$$

where F_b is the area of a single shear band in each element, and F_e is the area of the element.

8.2.3 *Simulation results*

The displacement obtained by the finite element analysis showed significantly different behaviours between the two types of soil bag model with features that are consistent with those obtained experimentally from the shaking-table test. This shows that finite element analysis that takes into account the main soil parameter characteristics and using plastic modelling can successfully simulate the actual behaviour of the dam. The soil parameters used in finite-element analysis were determined by simulation of direct shear tests on multi-layered soil bags, as listed in Table 4. Figure 40 shows simulation results of direct shear tests on multi-layered soil bags for the horizontal and inclined models. For stacked soil bag modelling, the soil bag was defined as elastic, and the interface between bags was assumed to behave as an elasto-plastic material. The prediction is good at the main points of interest, such as the shear strength and the vertical deformation (dilation of stacked bags). The finite element analysis successfully

Table 4. Material parameters

Material type	Elastic modulus (MN/m^2)	Poisson's ratio	Cohesion (kPa)	Internal friction angle (degrees)	Unit weight (kN/m^3)
Fill material	9.8	0.3	2.1	38.9	15.7
Soil bag	19.6	0.3	–	–	15.7
Interface	98	0.3	0	23.2	15.7

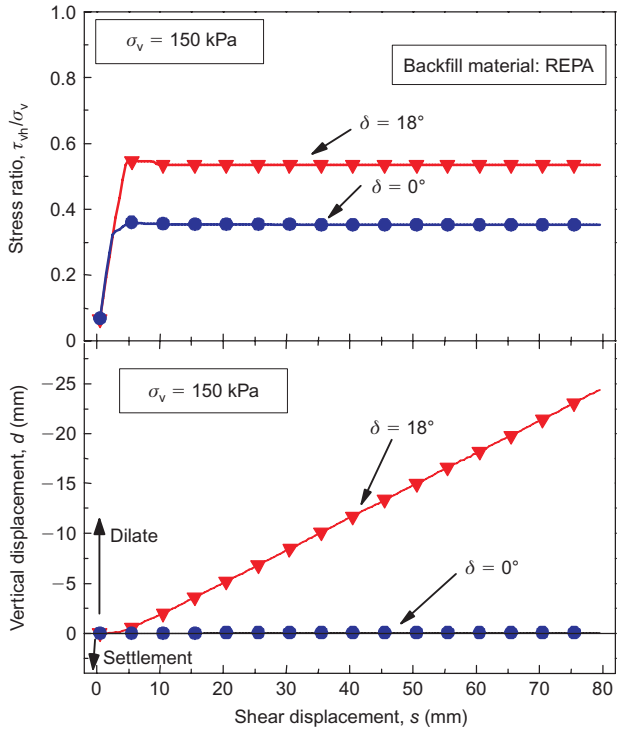

Figure 40. FE simulation for direct shear test of multi-layered stacked soil bags

simulated the sliding along the interface between stacked bags. The internal friction angle for the interface was 23.2° as defined by the direct shear test. Figure 41 shows the finite element mesh of the dam model with inclined soil bags stacked on the dam slopes (i.e. the inclined model) used for the analysis with elasto-plastic constitutive models. Figure 42 shows the settlement of the dam crest for the two models at each excitation. The inclined model settled down less during the shaking than the horizontal model. For greater shaking intensity (a_{max} = 7 m/s^2), the horizontal model settled at the crest five times

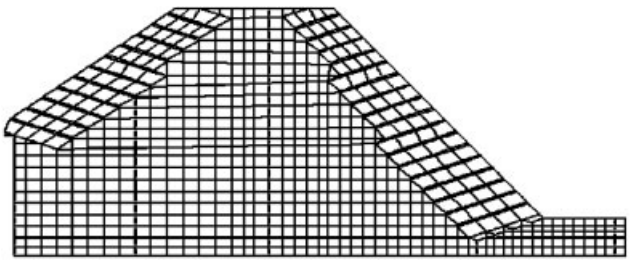

Figure 41. FE mesh for horizontal model, including stacked soil bags and interface

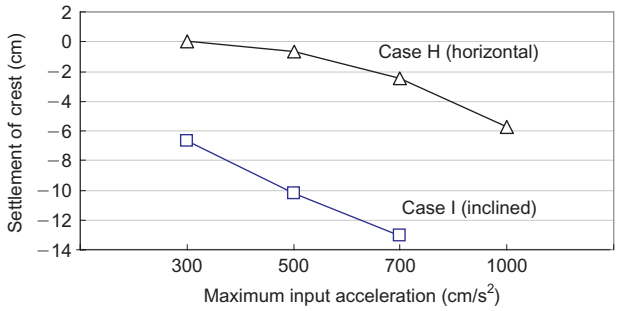

Figure 42. Simulation results of vertical settlement for GSET dam models (horizontally stacked and inclined stacked models), at each excitation level

more than the inclined model. This trend is similar to the experimental result shown in Figure 38.

Figure 43 shows the maximum shear strain distribution after shaking (a_{max} = 5 m/s^2). For the horizontal model, the maximum shear strain distribution of the embankment is concentrated in the backfill in the bottom zone of the soil bag wall, and propagates from the toe end of the

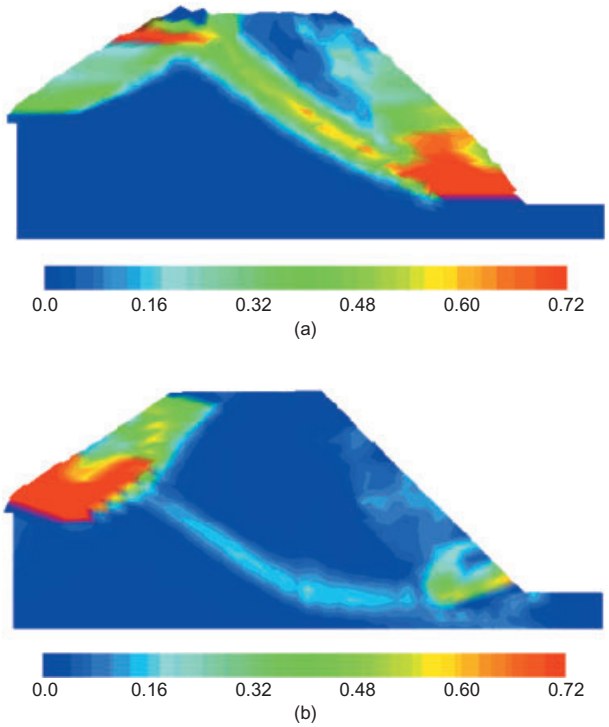

Figure 43. Maximum shear strain distribution for each model after a_{max} = 5 m^2/s excitation (a) horizontal model; (b) inclined model. Maximum shear strain is 80% for horizontal model and 20% for inclined model

downstream slope to the crest, contiguous with the back of the soil bag layer. For the inclined model, the maximum strain concentration is much less than for the horizontal model, and its distribution is in the embankment away from the soil bag wall, progressing from the toe end to the upstream slope. The finite element analysis was successful in simulating the experimentally observed sliding surface. From this finding it can be concluded that finite element analysis that takes into account the main soil parameter characteristics and uses plastic modelling can successfully simulate the real behaviour of GSET dams.

9. IN SITU TEST

NIRE constructed a full-scale earth fill embankment using GSET as shown in Figure 44, examined its construction performance, observed its behaviour during the construction, and conducted a test to evaluate the long-term durability of the model (Matsushima *et al.* 2006b; Yamazaki *et al.* 2006).

For this test, an embankment having two test sections was constructed, with a height of 3.2 m, an upstream slope of 1H:1.8H, a downstream slope of 1V:1H and a body width of 21 m. Kanto loam was used for the embankment material for both sections (Figure 44). A 10 m-wide section of the embankment was made of soil bags containing Kanto loam as type 1. In the other 11 m-wide section as type 2, recycled crushed concrete aggregate (RC-40 with $D_{max} = 40.0$ mm) was used as the backfill material for soil bags.

A screw extruder unit was developed for making soil bags, as shown in Figure 45. This machine makes it possible to produce bags on site which substantially improves construction performance, as it is not necessary to transport filled bags to site. After each bag was placed, it was fully compacted with a vibrator and stacked at a 15° angle in order to increase the shear strength of the stacked soil bags. Figure 46 shows the construction sequence for the GSET dam. The first geosynthetic soil bag layer is placed on the base foundation and compacted using a heavy roller compactor. Then the second layer is placed on the first layer and compacted in similar fashion. This procedure is repeated until the full height of the slope is completed.

Figure 45. Typical screw extruder for filling soil bags (after Mohri *et al.* 2007)

After the embankment was completed, it was used to retain water to conduct long-term observations of the behaviour of this earthfill dam. A maximum lateral displacement of ±10 mm was recorded immediately after construction for both the Type 1 and Type 2 dams, but both types then remained very stable for one year after construction, with a variation of ±5 mm or less, as shown in Figure 47. Figure 48 and Table 5 show the results of limit state analysis. For the embankment without soil bags, the factor of safety was 0.578 under static conditions. However, when the downstream slope was constructed with GSET to construct

Table 5. Limit state analysis for soil bag system

Type	Factor of safety	
	Static	Seismic
Normal embankment	0.578	0.461
GSET embankment	1.736	1.491

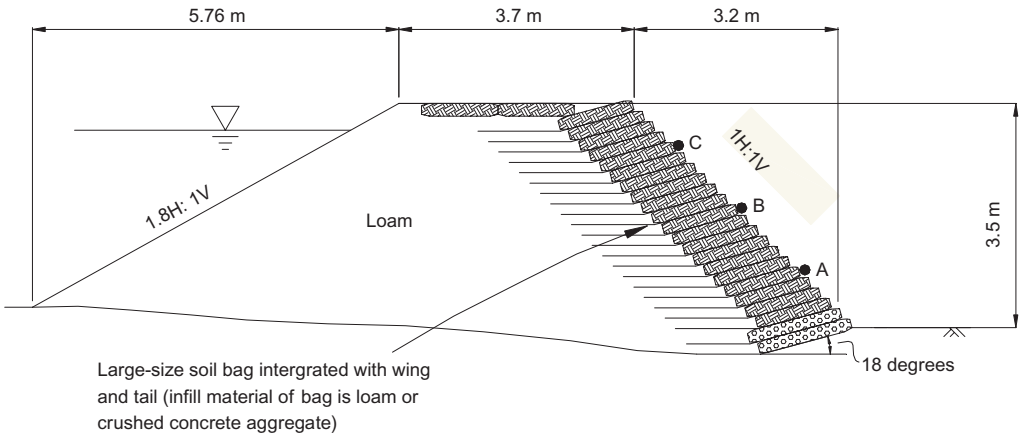

Figure 44. Cross-section of in situ test for GSET dam (surface displacement by laser profiler at points A, B and C)

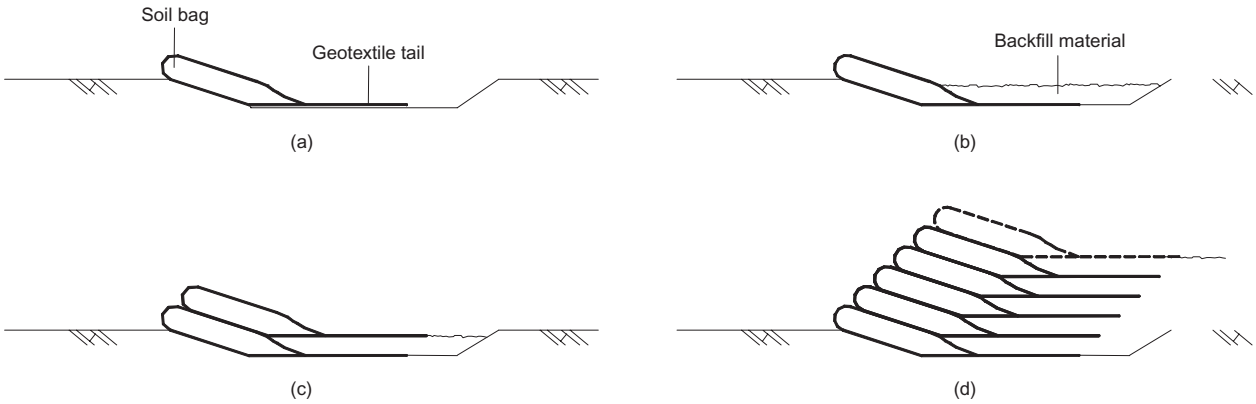

Figure 46. Construction process for GSET dam (after Huang *et al.* 2008): (a) laying soil bag with tail; (b) backfill and compaction; (c) second layer; (d) process repeated

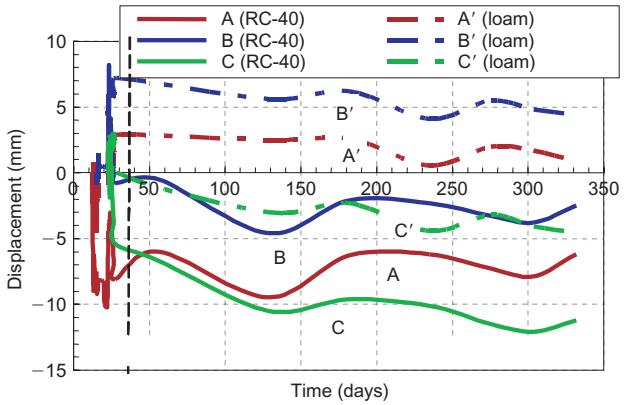

Figure 47. Lateral displacement of soil bag surface after construction (surface displacement by laser profiler at points A, B and C in Figure 44) (Yamazaki *et al.* 2006)

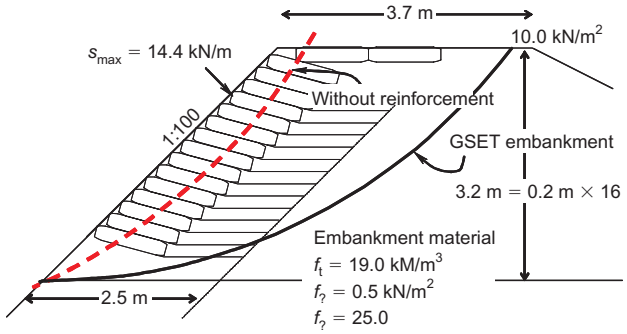

Figure 48. Limit state analysis for soil bag system (Yamazaki *et al.* 2006)

the embankment, the factor of safety was increased to 1.736. Even during an earthquake the dam stabilised by using stacked inclined soil bags exhibited a factor of safety of 1.491.

In this test, the embankment was overlaid with soil-cement or vegetation as shown in Figure 49, in order to confirm the effectiveness and durability of these methods for preventing ultraviolet deterioration of soil bags.

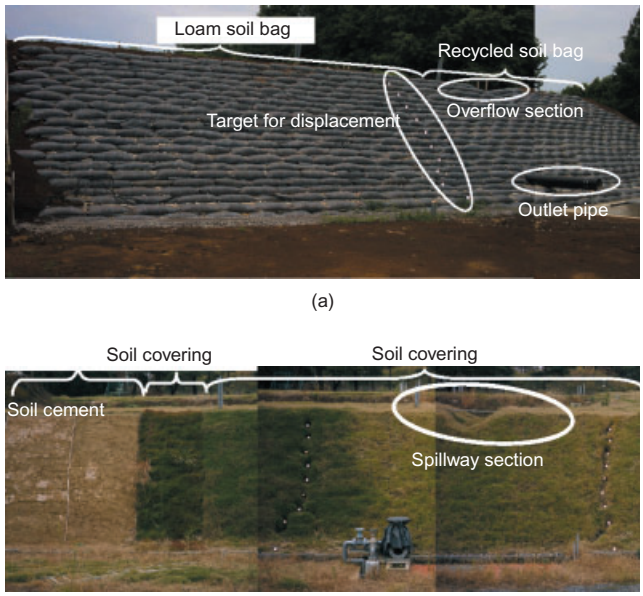

Figure 49. Surface of dam: (a) after piling up soil bags; (b) overlain with soil-cement and vegetation

10. CONCLUSIONS

A large number of small earthfill dams for agricultural irrigation, with an embankment height of 15m or less, were either damaged or failed completely during recent severe earthquakes, or during overflow in flooding events that exceeded the drainage capacity of the spillway discharge system. This paper has focused on the development of a new construction method for small earthfill dams.

A high-performance earthfill dam, which can tolerate overflow due to flooding and has increased earthquake resistance, is realised by using geosynthetic soil bags with extended wing and tail (GSET) to construct the dam dyke. The mechanical behaviour of stacked GSET embankments have been described.

The following conclusions can be drawn from the test results presented in this paper.

(1) The compressive strength of stacked soil bags depends on the infill material used. Soil bags filled with crushed concrete aggregate are more stable, and their behaviour is stiffer, than bags filled with finer material. Preloading of the soil bags is effective in reducing creep deformation, as well as increasing the stiffness at small deformations.
(2) The shear strength of stacked soil bags is low when they are sheared horizontally, because the interface between adjacent soil bags has a low friction angle compared with the infill materials. Inclined stacking of the soil bags increases the shear strength against lateral loading.
(3) In terms of dynamic behaviour, the results from shaking-table tests reveal that a GSET dam having a stack of inclined soil bags can exhibit a high seismic stability. The dam model showed a large vertical settlement of 304 mm at the crest, but there was no failure of the stacked soil bags or embankment.
(4) Breaching tests for soil bag embankments were performed with large soil bags (GSET). The soil bags were not damaged by the impact of flood water, and this embankment was still very stable, even when the overflow depth increased to 0.323 m. After artificial damage of the soil bag surface by cutting, some of the backfill material was released as the damage expanded. Nevertheless, there was no overall collapse of the downstream slope of the embankment during overflow testing for a total period of 150 min with an overflow depth of 0.583 m.
(5) The results of finite-element analysis were consistent with the experimental results. In particular, the failure plane pattern obtained by numerical analysis was similar to the test results.

In summary, the proposed system for construction and rehabilitation of new and existing dams with GSET is a very cost-effective technology to achieve high stability and safety against earthquakes and overflow due to heavy rainfall.

ACKNOWLEDGEMENTS

The authors would like to express their appreciation to the committee members for IS-Kyushu 2007 for their cooperation, and wish to extend special thanks to J. Otani and Y. Miyata. U. Aqil assisted in the laboratory study. The assistance of A. Goran is also gratefully acknowledged.

NOTATIONS

Basic SI units are given in parentheses.

a amplitude of acceleration (m/s^2)
a_{max} maximum input acceleration (m/s^2)
c cohesion (Pa)
C damping matrix (dimensionless)
D_{50} mean particle diameter (m)
d_c critical depth (m)
D_{max} maximum particle size of backfill material (m)
D_r relative density (dimensionless)
F external force vector (N/m)
f yield function (Pa)
F_b area of a single shear band in each element (m^2)
F_e area of the element (m^2)
G_s specific gravity (dimensionless)
H average initial height of soil bag (m)
h_0 overflow depth on upstream side of crest (m)
h_1 overflow depth on centre of crest (m)
I_1 first invariant (positive in tension) of deviatoric stresses (Pa)
L average initial height of soil bag (m)
L/H aspect ratio of soil bag (dimensionless)
m, ε_f, ε_r material constants (dimensionless)
M_D diagonalised mass matrix (dimensionless)
N_δ normal force on stacked plane (N)
P force vector (N/m)
P_h lateral shear force (N)
P^{init} nodal forces due to initial stresses (Pa)
P_v vertical force (N)
q discharge unit quantity flow (m^3/s/m)
q_n displacement vector at time n (m/m)
S lateral displacement of top loading platen (m)
s shear displacement (m)
T_δ shear force on stacked plane (N)
Δt time increment (s)
U_c coefficient of uniformity (dimensionless)
υ velocity vector (m/s)
W average initial width of soil bag (m)
w_{opt} optimum water content (dimensionless)
α_{damp} damping ratio (dimensionless)
α_p value of α at peak state (dimensionless)
α_r value of α in residual state (dimensionless)
δ inclination angle of stacked soil bags (degrees)
$\varepsilon_{v,ave}$ average axial strain (positive in compression) (dimensionless)
θ_L Lode angle (degrees)
ν Poisson's ratio (dimensionless)
ρ_{dmax} maximum dry unit weight (N/m^3)
σ_n normal stress on stacked plane (Pa)
σ_v vertical stress (Pa)
$\sigma_{v,ave}$ average axial stress (positive in compression) (Pa)
$\overline{\sigma}$ second invariant of deviatoric stress (Pa)
τ_n shear stress on stacked plane (Pa)
τ_{vh} lateral shear stress (Pa)
τ_{vh}/σ_v stress ratio (dimensionless)
Φ plastic potential function (Pa)
ϕ internal friction angle of backfill (degrees)
ϕ_r residual friction angle (degrees)
ϕ_{sb} interface friction angle between interfaces of soil bags (degrees)
ψ dilatancy angle (degrees)

REFERENCES

Aqil, U., Matsushima, K., Lohani, T. N., Mohri, Y., Yamazaki, S. & Tatsuoka, F. (2005). Large scale shearing tests of stacked soil bags.

Proceedings of the 40th Annual Conference on Geotechnical Engineering, Sapporo, Japan, Vol. 40, pp. 735–736.

Aqil, U., Matsushima, Mohri, Y., Yamazaki, S. & Tatsuoka, F. (2006). Lateral shearing tests on geosynthetic soil bags. *Proceedings of the 8th International Conference on Geosynthetics*, Hachinohe, Japan, pp. 1703–1706.

Arangelovski, G., Mohri, Y., Matsushima, K. & Yamazaki, S. (2006). Comparison of analytical and experimental residual displacement of an earth dam improved with geotextile soil bag system. *Proceedings of the 41th Annual Conference on Geotechnical Engineering,* Kagoshima, Japan, pp. 689–690.

Bathurst, R. J. & Hatami, K. (1998). Seismic response analysis of geosynthetic reinforced soil retaining wall. *Geosynthetics International*, **5**, No. 1–2, 127–166.

Cho, S. M., Jeon, B. S., Park, S. I. & Yoon, H. C. (2008). Geotextile tube application as the cofferdam at the foreshore with large tidal range for Incheon bridge project. *Proceedings of the 4th Asian Regional Conference on Geosynthetics*, Shanghai, China, pp. 591–596.

Chen, G. L., Huang, Y., Sato, M. & Chida, S. (2008). Application of stacked soilbags for slope protection. *Proceedings of the 4th Asian Regional conference on Geosynthetics*, Shanghai, China, pp. 609–614.

Dodge, R. A. (1988). *Overtopping Flow on Low Embankment Dams: Summary Report of Model Tests*. REC-ERC-88-3, US Bureau of Reclamation, Denver, CO, USA, 28 pp.

Fujii, H., Shimada, K. & Nishimura, S. (1991). *Damage to Small Earthfill dam in Okayama Pref. at Typhoon 19th in 1990.* Final Report of Grants-in-Aid for Scientific Research, Ministry of Education, Culture, Sports, Science and Technology, Tokyo, Japan, pp. 101–130 (in Japanese).

Ghazali, N. H. M., Kam, S. & Yee, T. W. (2006). Geotextile tube for protection of mangrove coast at Tanjung Piai Johor National Park, Malaysia. *Proceedings of the 8th International Conference on Geosynthetics,* Yokohama, Japan, pp. 773–776.

Hori, T., Tagashira, H., Yasunaka, M. & Tani, S. (1998). Damage to earth dams in 1997. *Proceedings of the 8th International Congress of the International Association of Engineering Geology*, Vancouver, Canada, pp. 241–248

Hyogo Pref. (1996). *Final Report for 1995 Hyogoken Nanbu Earthquake*. Department of Agriculture of Hyogo Prefecture, pp. 81–83.

Huang, C. C., Matsushima, K., Mohri, Y. & Tatsuoka, F. (2008). Analysis of sand slopes stabilized with facing of soil bags with extended reinforcement strips. *Geosynthetics International*, **15**, No. 4, 232–245.

Hubert, C. (1994). *Hydraulic Design of Stepped Cascades, Channels, Weirs and Spillways*, 1st edn. Pergamon, Oxford.

Kim, M., Freeman, M., FitzPatrick, B. T., Nevius, D. B., Plaut, R. H. & Filz, G. M. (2004). Use of an apron to stabilize geomembrane tubes for fighting floods. *Geotextiles and Geomembranes*, **22**, No. 4, 239–254.

Krahn, T., Blatz, J., Alfaro, M. & Bathurst, R. J. (2007). Large-scale interface shear testing of sandbag dyke materials. *Geosynthetics International*, **14**, No. 14, 119–126.

Lawson, C. R. (2008). Geotextile containment for hydraulic and environmental engineering. *Geosynthetics International*, **15**, No. 6, 384–427.

Leshchinsky, D., Leshchinsky, O., Ling, H. I. & Gilbert, P. A. (1996). Geosynthetic tubes for confining pressurized slurry: some design aspects. *Journal of Geotechnical Engineering Division, ASCE*, **122**, No. 8, 682–690.

Lohani, T. N., Matsushima, K., Mohri, Y. & Tatsuoka, F. (2004). Stiffness of soil bags filled with recycled concrete aggregate in compression. *Proceedings of the International Conference on Geosynthetics and Geoenvironmental Engineering*, Bombay, India, pp. 106–112.

Lohani, T. N., Matsushima, K., Aqil, U., Mohri, Y. & Tatsuoka, F. (2006). Evaluating the strength and deformation characteristic of a soil bag pile from full-scale laboratory tests. *Geosynthetics International*, **13**, No. 16, 246–264.

Maruyama, N., Murayama, M. & Sasaki, F. (2006). Construction of a geogrid-reinforced counter-weight fill to increase the seismic stability of an existing earth dam. *Proceedings of the 8th International Conference on Geosynthetics*, Yokohama, Vol. 2, pp. 643–646.

Matsuoka, H., Hasebe, T., Liu, S. H. & Shimao, R. (2003). Friction property of soilbags and some measures to increase soil bag resistances against sliding. *Proceedings of the 38th Annual Symposium on Geotechnical Engineering*, Akita, Japan, pp. 869–870 (in Japanese).

Matsuoka, H., Liu, S. H. & Yamaguchi, K. (2001). Mechanical properties of soilbags and their application to earth reinforcement. *Proceedings of the International Symposium on Earth Reinforcement*, Fukuoka, Japan, Vol. 1, pp. 587–592.

Matsushima, K., Yamazaki, S., Mohri, Y. and Arangelovski, G. (2005). Overflow model test of small dam with soil bag. *Proceedings of the 40th Annual Symposium on Geotechnical Engineering*, Hakodate, Japan, pp. 1995–1996 (in Japanese).

Matsushima, K., Mohri, Y., Aqil, U., Aranglovski, G., Hironaka, J. & Yamazaki, S. (2006a). Shaking table model test on small earth dam with geotextile soil bags. *Proceeding of the 41th Annual conference on Geotechnical Engineering*, Kagoshima, Japan, pp. 685–686 (in Japanese).

Matsushima, K., Yamazaki, S., Mohri, Y., Aqil, U. & Tatsuoka, F. (2006b). Structural features of earth dams allowing overtopping and a full-scale construction test. *Proceedings of the Annual Symposium on Irrigation, Drainage and Reclamation Engineering*, Utsunomiya, Japan, CD-ROM (in Japanese).

Matsushima, K., Yamazaki, S., Mohri, Y., Hori, T., Ariyoshi, M. & Tatsuoka, F. (2007). Large-scale overflow-induced collapse tests on embankments using soil bags anchored with geosynthetic-reinforcements. *Proceedings of the International Symposium on Earth Reinforcement, IS Kyushu '07*, Fukuoka, Japan, pp. 881–888.

Matsushima, K., Aqil, U., Mohri, Y. & Tatsuoka, F. (2008). Shear strength and deformation characteristics of geosynthetic soil bags stacked horizontal and inclined. *Geosynthetics International*, **15**, No. 2, 119–135.

Mohri, Y., Matsushima, K., Hori, T. & Tani, S. (2005). Damage to small-size reservoirs and their reconstruction method. *Foundation Engineering and Equipment* (Kiso-ko), Special Issue on Lessons from the 2004 Niigata-ken Chu-Etsu Earthquake and Reconstruction, October, pp. 62–65 (in Japanese).

Mohri, Y., Matsushima, K., Yamazaki, S., Lohani, T. N., Goran, A. & Aqil, U. (2007). New direction of earth reinforcement: disaster prevention. *Proceedings of the International Symposium on Earth Reinforcement, IS Kyushu '07*, Fukuoka, Japan, pp. 85–101.

Powledge, G. R., Ralston, D. C., Miller, P., Chen, Y. H., Clopper, P. E. & Temple, D. M. (1989a). Mechanics of overflow erosion on embankments. I: Research activities. *Journal of Hydraulic Engineering*, **115**, No. 8, 1040–1055.

Powledge, G. R., Ralston, D. C., Miler, P., Chen, Y. H., Clopper, P. E. & Temple, D. M. (1989b). Mechanics of overflow erosion on embankments. II: Hydraulic and design considerations. *Journal of Hydraulic Engineering*, **115**, No. 8, 1056–1075.

Ralston, D. C. (1987). Mechanics of embankment erosion during overflow. *Proceedings of the 1987 ASCE National Conference on Hydraulic Engineering*, Williamsburg, VA, USA, pp. 733–738.

Tani, S. (1996). Damage to earth dams. *Soil and Foundations*, Special issue on geotechnical aspects of the 17 January 1995 Hyogoken–Nambu earthquake, January, 263–273.

Tatsuoka, F., Tateyama, M., Uchimura, T. & Koseki, J. (1997). Geosynthetic-reinforced soil retaining walls as important permanent structures. 1996–1997 Mercer Lecture, *Geosynthetics International*, **4**, No. 2, 81–136.

Tatsuoka, F., Koseki, J., Tateyama, M., Munaf, Y. & Matsushima, K. (1998). Seismic stability against high seismic loads of geosynthetic-reinforced soil retaining structures. *Proceedings of the 6th International Conference on Geosynthetics*, Atlanta, GA, USA, Vol. 7, pp. 103–142.

Tatsuoka, F., Tateyama, M., Mohri, Y. & Matsushima, K. (2007). Remedial treatment of soil structures using geosynthetic-reinforcing technology. *Geotextiles and Geomembranes*, **25**, No. 4, 204–220.

Temple, D. M. (1989). Mechanics of an earth spillway failure. *Transactions of the ASAE*, **32**, No. 6, 2015–2021.

Tournier, J. P. (2006). *Safety of Fill Dams*. The International Commission on Large Dams, Paris, France, General Report Q86, pp. 1327–1381.

Yamazaki, S., Matsushima, K., Mohri, Y. & Arangelovski, G. (2006). Prototype test of small dam with soil bag. *Proceeding of the 41th Annual Conference on Geotechnical Engineering*, Kagoshima, Japan, pp. 1825–1826 (in Japanese).

Yasuda, Y. & Ohtsu, I. (1999). Flow resistance of skimming flows in stepped channels. *Proceedings of the 28th IAHR Congress*, Graz, Austria, Session B14 (CD-ROM).

Yasunaka, M. & Tagashira, H. (1994). Damage and rehabilitation for small earth fill dam by heavy rain fall and earthquake. *Drainage and Reclamation Engineering*, **32**, 33–44 (in Japanese).

Xu, Y. F. & Huang, J. (2008). Case study on earth reinforcement using soilbags. *Proceedings of the 4th Asian Regional Conference on Geosynthetics*, Shanghai, China, pp. 597–602.

The Editor welcomes discussion on all papers published in Geosynthetics International. Please email your contribution to discussion@geosynthetics-international.com by 15 February 2010.